
Article:
Vajpayee, V. orcid.org/0000-0003-1179-7118, Becerra, V., Bausch, N. et al. (3 more authors) (2020) Dynamic modelling, simulation, and control design of a pressurized water-type nuclear power plant. Nuclear Engineering and Design, 370. 110901. ISSN 0029-5493

https://doi.org/10.1016/j.nucengdes.2020.110901

Dynamic Modelling, Simulation, and Control Design of a Pressurized Water-type Nuclear Power Plant

Vineet Vajpayee, Victor Becerra, Nils Bausch, Jiamei Deng, S. R. Shimjith, A. John Arul

***Abstract*—This article presents an integrated non-linear dynamic model of a Pressurized Water-type Nuclear Reactor (PWR) and associated plant components for control design and evaluation purposes. The model uses the first-principles approach to represent various components of the plant. The model considers the dynamics of the reactor core, thermal hydraulics, piping and plenum, pressurizer, steam generator, condenser, and turbine-governor system, in addition to various actuators and sensors. The response of the proposed model is tested using perturbations in different input variables. Various control loops implementing low-level PI control strategies are designed and implemented in the model to simulate the closed-loop behaviour of the plant. These include control loops for reactor power, steam generator pressure, pressurizer pressure and level, and turbine speed. Linear quadratic Gaussian-based optimal control strategies are further developed and implemented. Unique contributions of the work include the set of plant sections that are considered, the implementation of carefully tuned control strategies, the completeness of the model equations, and the availability of parameter values so that the model is readily implementable and has the potential to become a benchmark for control design studies in PWR nuclear power plants.**

***Index Terms*—Mathematical Model, Simulation, Control System, Optimal Control, Pressurized Water Reactor, Nuclear Power Plant.**

NOMENCLATURE

A_p	Cross-sectional area of pressurizer (m^2)
C	Delayed neutron precursor concentration
C_{tg}	Turbine governor valve coefficient
C_{heat}	Thermal conductance $(J/m.^0C)$
G	Reactivity worth $(cent/step)$
H	Rate of rise of temperature $(^0Cs^{-1})$
I	Moment of inertia $(kg.m^2)$
J	Conversion factor
K	Gain
P	Power $(per\ unit)$
Q_{heat}	Rate of heat addition (kW/s)
R_{heat}	Thermal resistance $(m^0.C/W)$
S	Effective heat transfer area (m^2)
T	Average temperature (^0C)
U	Heat transfer coefficient $(W/m^2.^0C)$
V	Volume (m^3)
c_p	Specific heat $(J/kg.^0C)$
d	Density (kg/m^3)
h	Enthalpy (J/kg)
i	Current (mA)
l	Pressurizer length (m)
m	Mass (kg)
$\dot{m}$	Mass flow rate (kg/s)
p	Pressure (MPa)
v_{rod}	Rod speed (spm)
Λ	Neutron generation time (s)
α	Coefficient of reactivity $(^0C^{-1})$
β	Fraction of delayed neutrons
κ	Constant
λ	Decay constant (s^{-1})
ρ	Reactivity $(cents)$
ζ	Damping ratio
τ	Time constant (s)
ν	Specific volume (m^3/kg)
ω_{tur}	Turbine speed (Hz)
ϖ	Natural frequency of oscillation (rad/s)

Subscripts

$c1$, $c2$	Coolant at node 1 and 2
coh,cow,cos	Condenser hot-well, water, steam
f	Fuel
fw	Feed-water
$heat$	Heater
hot, $cold$	Hot and cold leg
hp, ip, lp,	High, intermediate, and low pressure steam
i	i^{th} group of delayed neutron precursor
lo, lr	Logarithmic and Log rate amplifier
$m1$, $m2$	MTL 1 and MTL 2
$mp1$, $mp2$	Transfer from MTL 1, 2 to PCL 1, 2
$ms1$, $ms2$	Transfer from MTL 1, 2 to SCL
n	Normalized values
p	Pressurizer
$p1$, $p2$	PCL 1 and PCL 2
$pm1$, $pm2$	Transfer from PCL 1, 2 to MTL 1 , 2
rod	Regulating rod
rxi, rxu	Reactor lower and upper plenum
s,ss	Steam, Steam in secondary
sg, sgi, sgu	Steam generator, inlet, and outlet plenum

Vineet Vajpayee (vineet.vajpayee@port.ac.uk), Victor Becerra (victor.becerra@port.ac.uk), and Nils Bausch (nils.bausch@port.ac.uk) are with School of Energy and Electronic Engineering, University of Portsmouth, Portsmouth, PO1 3DJ, United Kingdom.

Jiamei Deng (j.deng@leedsbeckett.ac.uk) is with School of Built Environment, Engineering, and Computing, Leeds Beckett University, Leeds, LS6 3QS, United Kingdom.

S. R. Shimjith (srshim@barc.gov.in) is with Reactor Control System Design Section, Bhabha Atomic Research Centre, Mumbai, 400 085, India and Homi Bhabha National Institute, Mumbai, 400 094, India.

A. John Arul (arul@igcar.gov.in) is with Probabilistic Safety, Reactor Shielding and Nuclear Data Section, Indira Gandhi Centre for Atomic Research, Kalpakkam, 603 102, India.

spr, sur	Spray and surge
$rtd1$, $rtd2$	RTD 1 and 2
tg	Turbine-Governor
tur	Turbine
w,ws,wo	Water, Secondary, Outlet,

I. Introduction

Development of a mathematical model for a nuclear power plant to comprehend the underlying behaviour of associated processes is a challenging task. Modelling of different subsystems in a nuclear power plant is required for various purposes including retrofitting new devices, analysing the effects of faults and other disturbances, controller design and tuning, and optimisation of the plant operation. Accurate mathematical modelling of the dynamics of the plant is of prime importance due to the fact that it plays a significant role in control systems design, fault diagnosis & isolation, prediction, and in ascertaining long-term safe operation of a nuclear power plant. For instance, control of reactor temperature or power is a decisive factor in assuring stable and planned performance of a nuclear power plant. In terms of control operation, the design and analysis of control loops necessitate a fairly accurate and simple model of a nuclear power plant as the control performance is mainly decided by the considered model. In most of the model-based approaches, achievement of design objective is predominantly decided by the accuracy of the employed model. Thus, it is important to arrive at a plant model which is reasonably accurate and at the same time simple enough to achieve the design objectives.

Generally, the mathematical model of a nuclear power plant is derived either from the first principles approach using fundamental laws of physics or from the system identification approach. In the first principles approach, the dynamics of nuclear reactors can be illustrated using a time-dependent Boltzmann transport model [1]. Nonetheless, its use coupled with delayed neutron precursors' model is inconvenient for practical purposes. These problems can be solved with approximate methods such as time-dependent group diffusion equations. The simplest form derived from the original Boltzmann equation is known as the Point Kinetics (PK) reactor model. It assumes that production, diffusion, absorption, and leakage of neutrons take place at single energy independent of space variables. The PK model has been mainly used by researchers to develop control strategies. For instance, recently Subudhi et al. [2] developed a total reactor power control scheme for a Pressurized Heavy Water-type Reactor (PHWR) employing the PK model. For large PHWRs, nodal method-based approximated core neutronics models are formulated from neutron diffusion equation [3], [4]. However, the dynamics of neutron flux detector, associated amplifier, reactivity devices and core thermal hydraulic have been ignored. In case of Pressurized Water-type Reactor (PWR), lumped parameters models of different subsections have been proposed in the literature using ordinary differential equations. In the earliest work, Freels [5] demonstrated linear simulation of a PWR. The primary loop non-linear modeling of a PWR is presented by Mneimneh [6]. Ali [7] presented different mathematical models for the Steam Generator (SG) based on lumped parameter technique. Thakkar [8] discussed a theoretical model of a pressurizer to predict dynamic behaviour in transient as well as in steady state conditions. Some control oriented pressurizer models can be found in the literature [9]–[11]. Kerlin et al. [12], [13] demonstrated the model behaviour to step disturbances and compared with actual measurement obtained from H. B. Robinson nuclear power plant. A similar modeling approach has been utilized by Arda et al. [14], [15] to develop analytical models of a passively cooled small modular reactor. A lumped parameter approach based non-linear modeling has been adopted by Masoud [16] for performing computer simulation of a PWR system. In a recent work, a non-linear mathematical model of a nuclear steam supply system comprising of reactor core and SG dynamics is built by Wan et al. [17].

In contrast, empirical modelling or system identification is another approach for developing systematic dynamical models from collected measurements data. It has been applied by some researchers to model and validate different sections of a nuclear power plant. Validation of a theoretical model with experimental data for flux mapping is performed by Pomerantz et al. [18]. A linear dynamic model of a fluidized bed nuclear reactor is proposed by Lathouwers et al. [19]. Venter et al. [20] applied system identification approach to derive mathematical model of a simulation of the pebble bed modular reactor. Fazekas et al. [21] modelled the primary loop of VVER-type nuclear reactor for control requirements. Gabor et al. [22] discussed system identification of a LTI state-space model of a VVER-type nuclear reactor. Das et al. [23] used system identification to develop plant model around different operating points during step-back transients. Sohn et al. [24] utilized system identification to build a simplified SG model for designing the feed-water control system.

In other recent works, the empirical modelling approach has been combined with soft-computing techniques. Kim et al. [25] estimated parameters of PWR cores using Artificial Neural Network (ANN) models. Recurrent neural network based algorithms have been proposed to identify reactor core models [26], [27]. Boroushaki et al. [28] combined a non-linear autoregressive with exogenous input model structure with ANN for the core identification of a VVER-type nuclear reactor and the identified model is used in predicting the behaviour of reactor dynamics. Pressurizer model for a PWR is developed based on the feed-forward back propagation ANN [29]. Khalafi et al. [30] developed a research reactor simulator using an identified ANN model. A neuro-fuzzy model-based identification technique has been applied to predict water-level in the SG of a PWR [31]. In most of the reported works, the reactor is considered as a LTI process evolving at single-scale. An heuristic approach based on multi-scale system identification has been recently developed [32], [33].

Most of the nuclear power plant modelling work reported in the literature to date either represents a specific subsystem of the nuclear power plant [2], [21]–[28] or when a complete model is given, it is normally too complex for control design purposes [7], [14]–[16], [34]. To the best of the authors knowledge, none of the aforementioned works [2], [7],

[14]–[16], [21]–[28], [34] present a complete implementable nuclear power plant model for control design. And yet, a complete but simple plant model is needed by researchers and engineers for the purpose of control systems design and evaluation. PWR simulators such as PCTRAN containing models of major plant systems are made available by IAEA [35]. Other simulators based on thermal-hydraulics codes such as RELAP5 [36], APROS [37] are also used to verify and validate behaviour of developed plant models. However, it is difficult to replace the existing control algorithms or to plug in user designed controllers/observers. The present work is an attempt to address the control-oriented modelling problem. In many control applications, it is preferable to cast the plant model equations as a set of first-order differential equations so that they can be expressed in standard state-space form. The main goal of the proposed work is to present a simple yet complete integrated non-linear model of a PWR-type nuclear power plant for control system design and simulation purposes. The nuclear power plant model presented in the paper is of a typical Westinghouse-type PWR configuration with 1.2 GW electrical capacity. The model captures information on the components available from the literature associated with PWR plants, Westinghouse documentation [38] and thermodynamic tables [39]. The PWR nuclear power plant consists of two loops, the primary loop and the secondary loop. The proposed model integrates the dynamics of the primary loop which includes reactor core, thermal-hydraulics, piping, plenum, steam generator, pressurizer, and the secondary loop which includes turbine, governor, reheater, and condenser. The model also contains various sensors and actuators. The integrated model effectively encompasses the dynamic behaviour of the PWR nuclear power plant and it is suitable for controller/observer design.

Another goal of the paper is to design and implement all the relevant nuclear power plant control loops to analyse the closed-loop performance of the proposed model. In literature, often, the coupling effects among the reactor-core, steam generator, pressurizer, turbine-governor, and different piping and plenum are ignored while designing the individual controllers. It is meaningful to develop control methods for the whole system. However, there are very few results available to control an entire plant. The proposed model represents well the qualitative behaviour of a PWR-type nuclear power plant thereby making it suitable for designing and testing control strategies. Moreover, with transient simulations being an integral part of the control system design and analysis task, the integrated model further establishes their relevance in advanced control design. Classical PI-based control and optimal Linear Quadratic Gaussian (LQG) control strategies are designed after proper tuning to analyse the closed-loop performance. Control strategy for core neutronics power control, temperature control, SG pressure control, pressurizer pressure control using heater and spray, pressurizer level control and turbine speed control loops are designed. The efficacy of the proposed work has been tested using various open and closed loop simulations in MATLAB/Simulink environment. The main contributions of the paper are listed below:

- Modelling of different integrated subsections of a PWR-type nuclear power plant, actuators, and sensors.
- Design of control loops for power, steam generator pressure, pressurizer pressure and level, and turbine speed.
- Carefully tuned PI and LQG control strategies for various scenarios across different control loops.
- Completeness of model equations, availability of parameter values, and comprehensive open and closed-loop analysis make the proposed model readily implementable.

The remainder of the paper is organized as follows: Section II presents the mathematical model. Section III presents the models of sensors and actuators. Section IV analyses different aspects of the system. Section V designs all the relevant control loops utilizing the model and discusses PI control strategies. Section VI presents the design of LQG control scheme. Section VII demonstrates the dynamic response for perturbation in different input variables. Section VIII presents the performance of the designed controllers. Finally conclusions are drawn in Section IX.

II. Non-linear Dynamic Model

A block diagram of the PWR-type nuclear power plant depicting interconnections of various systems is shown in Fig. 1. The heated coolant flows out of the upper plenum to the SG through the hot-leg (riser) to transfer heat from primary side system to secondary system. In the SG, the coolant enters through inlet plenum and then moves to the secondary node and comes out from the outlet plenum. The coolant is then fed-back to the reactor core through the cold-leg (downcomer) using recirculation pump to repeat the cycle. The secondary coolant coming out of the SG as superheated steam is fed to the turbine to generate mechanical power. The secondary coolant is then passed to condenser to remove the remaining heat. The liquid phase secondary coolant is pumped backs as feed-water to the SG to complete the power cycle [1].

A. Point Kinetics Reactor Core Model

The dynamic model of a PK nuclear reactor coupled with six-groups of delayed neutron precursor is considered. Effects of variation in temperatures of fuel and coolants and pressure of primary coolant system are considered in terms of reactivity feedback. The PK model is given by,

$$\frac{dP}{dt} = \frac{\rho_t - \sum_{i=1}^{6} \beta_i}{\Lambda} P + \sum_{i=1}^{6} \lambda_i C_i, \tag{1}$$

$$\frac{dC_i}{dt} = \frac{\beta_i}{\Lambda} P - \lambda_i C_i, \qquad i = 1, 2, \ldots 6. \tag{2}$$

From (1) and (2), the power and delayed neutron precursor concentration are normalized with respect to their respective full power values. Thus, the normalized PK model is given by,

$$\frac{dP_n}{dt} = \frac{\rho_t - \sum_{i=1}^{6} \beta_i}{\Lambda} P_n + \sum_{i=1}^{6} \frac{\beta_i}{\Lambda} C_{in}, \tag{3}$$

$$\frac{dC_{in}}{dt} = \lambda_i P_n - \lambda_i C_{in}, \qquad i = 1, 2, \ldots 6. \tag{4}$$

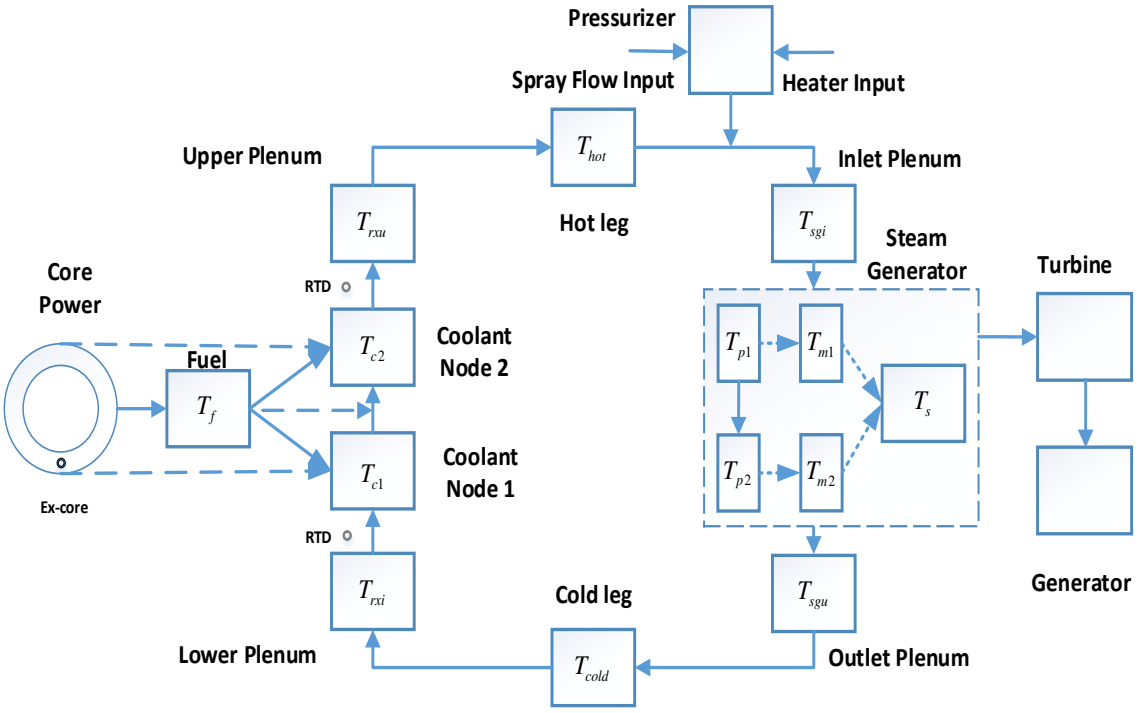

Fig. 1: Block diagram of different interconnected subsystems in a PWR nuclear power plant.

B. Thermal-Hydraulics Model

The core thermal-hydraulics model is given by Mann's model which considered two lumps for representing coolant and one lump to denote the fuel node [12]. It relates the core power to the temperature drop from fuel to coolant nodes. The model can represents the heat transfer better than the single coolant node approach. The model equations can be obtained by applying energy conservation to fuel and coolant volumes. The model is given by,

$$\frac{dT_f}{dt} = H_f P_n - \frac{1}{\tau_f}\left(T_f - T_{c1}\right), \tag{5}$$

$$\frac{dT_{c1}}{dt} = H_c P_n + \frac{1}{\tau_c}\left(T_f - T_{c1}\right) - \frac{2}{\tau_r}\left(T_{c1} - T_{rxi}\right), \tag{6}$$

$$\frac{dT_{c2}}{dt} = H_c P_n + \frac{1}{\tau_c}\left(T_f - T_{c1}\right) - \frac{2}{\tau_r}\left(T_{c2} - T_{c1}\right). \tag{7}$$

The above model assume that specific heat, density, and the heat transfer coefficient from fuel to coolant remain constant. The fluid flow is considered to be one-dimensional and the coolant nodes are assumed to be well stirred.

C. Piping & Plenum Model

Hot-leg (or riser) and cold-leg (downcomer), reactor lower and upper plenum and SG inlet and outlet plenum can be represented by first-order ordinary differential equations [12], [17]. It is assumed that the heat transfer takes place without any losses. The dynamic model is given by,

$$\frac{dT_{rxu}}{dt} = \frac{1}{\tau_{rxu}}\left(T_{c2} - T_{rxu}\right), \tag{8}$$

$$\frac{dT_{hot}}{dt} = \frac{1}{\tau_{hot}}\left(T_{rxu} - T_{hot}\right), \tag{9}$$

$$\frac{dT_{sgi}}{dt} = \frac{1}{\tau_{sgi}}\left(T_{hot} - T_{sgi}\right), \tag{10}$$

$$\frac{dT_{sgu}}{dt} = \frac{1}{\tau_{sgu}}\left(T_{p2} - T_{sgu}\right), \tag{11}$$

$$\frac{dT_{cold}}{dt} = \frac{1}{\tau_{cold}}\left(T_{sgu} - T_{cold}\right), \tag{12}$$

$$\frac{dT_{rxi}}{dt} = \frac{1}{\tau_{rxi}}\left(T_{cold} - T_{rxi}\right). \tag{13}$$

D. Steam Generator Model

A five node configuration is used to represent the SG in which, the Primary Coolant Lump (PCL), Metal Tube Lump (MTL), and Secondary Coolant Lump (SCL) are considered to have two, two, and one lump, respectively. It has been demonstrated by Ali [7] that this configuration would approximate the much complex SG model well enough and without increasing the complexity of the complete system. For PCL, it is assumed that specific heat and density are constants. For MTL, the thermal conductivity is assumed to be constant. The heat transfer coefficients during transients are also assumed to be constants. The fluid flow is considered to be one-dimensional

for both primary and secondary coolants [13], [15]. Based on these assumptions, the model is given by

$$\frac{dT_{p1}}{dt} = \frac{1}{\tau_{p1}}\left(T_{sgi} - T_{p1}\right) - \frac{1}{\tau_{pm1}}\left(T_{p1} - T_{m1}\right), \quad (14)$$

$$\frac{dT_{p2}}{dt} = \frac{1}{\tau_{p2}}\left(T_{p1} - T_{p2}\right) - \frac{1}{\tau_{pm2}}\left(T_{p2} - T_{m2}\right), \quad (15)$$

$$\frac{dT_{m1}}{dt} = \frac{1}{\tau_{mp1}}\left(T_{p1} - T_{m1}\right) - \frac{1}{\tau_{ms1}}\left(T_{m1} - T_{s}\right), \quad (16)$$

$$\frac{dT_{m2}}{dt} = \frac{1}{\tau_{mp2}}\left(T_{p2} - T_{m2}\right) - \frac{1}{\tau_{ms2}}\left(T_{m2} - T_{s}\right). \quad (17)$$

The equation of steam pressure for SCL can be obtained by balancing mass, volume, and heat which describes the two-phase mixture of liquid and saturated steam. The mass balances for water and steam are given by,

$$\frac{dm_{ws}}{dt} = \dot{m}_{fw} - \dot{m}_{sg}, \quad (18)$$

$$\frac{dm_{ss}}{dt} = \dot{m}_{sg} - \dot{m}_{so}. \quad (19)$$

The equation for volume balance is given by,

$$\frac{dV_{ws}}{dt} + \frac{dV_{ss}}{dt} = 0, \quad (20)$$

where $V_{ws} = m_{ws}\nu_{ws}$ and $V_{ss} = m_{ss}\nu_{ss}$. The heat balance equation is given by,

$$\frac{d\left(m_{ws}h_{ws}\right)}{dt} + \frac{d\left(m_{ss}h_{ss}\right)}{dt} = U_{ms1}S_{ms1}\left(T_{m1} - T_s\right) + U_{ms2}S_{ms2}\left(T_{m2} - T_s\right) + \dot{m}_{fw}c_{pfw}T_{fw} - \dot{m}_{so}h_{ss}. \quad (21)$$

Solving (18)–(22) gives,

$$\frac{dp_s}{dt} = \frac{1}{K_s}\left[U_{ms1}S_{ms1}\left(T_{m1} - T_s\right) + U_{ms2}S_{ms2}\left(T_{m2} - T_s\right) - \left(\dot{m}_{so}h_{ss} - \dot{m}_{fw}c_{pfw}T_{fw}\right)\right], \quad (22)$$

where

$$K_s = m_{ws}\frac{\partial h_{ws}}{\partial p_s} + m_{ss}\frac{\partial h_{ss}}{\partial p_s} - m_{ws}\left(\frac{h_{ws} - h_{ss}}{\nu_{ws} - \nu_{ss}}\right)\frac{\partial \nu_{ss}}{\partial p_s}. \quad (23)$$

It is considered that that feed-water inlet flow is adjusted to match steam outlet flow. Thus, (22) can be simplified as

$$\frac{dp_s}{dt} = \frac{1}{K_s}\left[U_{ms1}S_{ms1}\left(T_{m1} - T_s\right) + U_{ms2}S_{ms2}\left(T_{m2} - T_s\right) - \dot{m}_{so}\left(h_{ss} - c_{pfw}T_{fw}\right)\right]. \quad (24)$$

Under the assumption of critical flow in which the steam mass flow rate is considered to be dependent only on steam pressure, steam outlet flow is related to valve coefficient as

$$\dot{m}_{so} = C_{tg}p_s. \quad (25)$$

The temperature of SCL can be linearly approximated to steam pressure through rate of change in saturation temperature T_{sat} with respect to pressure as [12]

$$T_s = \frac{\partial T_{sat}}{\partial p_s}p_s. \quad (26)$$

E. Pressurizer Model

The purpose of a pressurizer is to accommodate changes in the reactor coolant volume due to changes in the temperature on the primary side. The pressurizer model consists of a mixture of liquid and vapour in equilibrium. It assumes that saturation conditions corresponding to primary coolant pressure are preserved at all times for water and steam mixture [15]. In surge flow mixes perfectly with the liquid inside the pressurizer. The vessel's wall and liquid surfaces are assumed to be free from condensation and there is no significant heat loss at the interface. It is assumed that the initial values of the spray flow rate and heater output do not have any effect on the model [6]. Further, steam compressibility is considered as a function of water and steam thermodynamic properties to represent pressure variations pragmatically [16]. The equation of water level can be obtained by applying mass balance equation on water and steam phase as,

$$\frac{dm_w}{dt} + \frac{dm_s}{dt} = \dot{m}_{sur} + \dot{m}_{spr}, \quad (27)$$

where $m_w = d_w A_p l_w$ and $m_s = d_s A_p (l - l_w)$. Solving (27),

$$\frac{dl_w}{dt} = \frac{1}{d_s A_p}\left(\left(A_p\left(l - l_w\right)K_{2p} - \frac{C_{2p}}{C_{1p}}\right)\frac{dp_p}{dt} + \frac{1}{C_{p1}^2}\left(C_{2p}\frac{dp_p}{dt} - \dot{m}_{sur} - \dot{m}_{spr}\right) + \frac{\dot{m}_{sur}}{C_{1p}}\right) \quad (28)$$

The two-phase dynamical model can be obtained by applying volume and energy balances of water and steam mixture with steam compressibility. They are given by,

$$\frac{dV_w}{dt} + \frac{dV_s}{dt} = 0 \quad (29)$$

where $V_w = m_w\nu_w$ and $V_s = m_s\nu_s$. This gives,

$$\frac{d\left(m_w(h_w - p_p\nu_w)\right)}{dt} + \frac{d\left(m_s h_{\bar{w}}\right)}{dt} + \frac{p_p}{J_p}\frac{dV_w}{dt} = Q_{heat} + \dot{m}_{sur}h_{sur} + \dot{m}_{spr}h_{spr}. \quad (30)$$

Simplifying (29)–(30),

$$\frac{dp_p}{dt} = \frac{Q_{heat} + \dot{m}_{sur}\left(\frac{p_p\nu_s}{J_pC_{1p}} + \frac{h_{\bar{w}}}{C_{1p}}\right) + \dot{m}_{spr}\left(h_{spr} - h_w + \frac{h_{\bar{w}}}{C_{1p}} + \frac{p_p\nu_w}{J_pC_{1p}}\right)}{m_w\left(K_{3p} + \frac{K_{4p}p_p}{J_p}\right) + \frac{m_sK_{4p}p_p}{J_p} - \frac{V_w}{J_p} + \frac{C_{2p}}{C_{1p}}\left(h_{\bar{w}} + \frac{p_p\nu_s}{J_p}\right)}. \quad (31)$$

The surge rate can be represented as,

$$\dot{m}_{sur} = \sum_{j=1}^{N} V_j\vartheta_j\frac{dT_j}{dt}, \quad (32)$$

where the index $j = 1$ to N represent coolant nodes in the following order, lower plenum, coolant node 1 and 2, upper plenum, hot-leg, inlet plenum, PCL 1 and 2 and outlet plenum, and cold-leg. The intermediate variables are defined as

$$C_{1p} = \frac{d_w}{d_s} - 1; C_{2p} = A_p\left(l - l_w\right)\frac{d_w}{d_s}K_{2p} + A_p l_w K_{1p};$$

TABLE I: Typical Parameters of a Westinghouse-type 1.2 GWe PWR Plant

$\lambda_1(s^{-1})$	$\lambda_2(s^{-1})$	$\lambda_3(s^{-1})$	$\lambda_4(s^{-1})$	$\lambda_5(s^{-1})$	$\lambda_6(s^{-1})$
1.2437×10^{-2}	3.05×10^{-2}	1.1141×10^{-1}	3.013×10^{-1}	1.12866	3.0130
β_1	β_2	β_3	β_4	β_5	β_6
2.15×10^{-4}	1.424×10^{-3}	1.274×10^{-3}	2.568×10^{-3}	7.48×10^{-4}	2.73×10^{-4}
$\Lambda(s)$	$H_f(^0Cs^{-1})$	$H_c(^0Cs^{-1})$	$\tau_f(s)$	$\tau_c(s)$	$\tau_r(s)$
3×10^{-5}	71.8725	1.1254	4.376	7.166	0.674
$\tau_{rxu}(s)$	$\tau_{rxi}(s)$	$\tau_{hot}(s)$	$\tau_{cold}(s)$	$\tau_{sgu}(s)$	$\tau_{sgi}(s)$
2.517	2.145	0.234	1.310	0.726	0.659
$\tau_{p1}(s)$	$\tau_{p2}(s)$	$\tau_{pm1}(s)$	$\tau_{pm2}(s)$	$\tau_{mp1}(s)$	$\tau_{mp2}(s)$
1.2815	1.2815	0.5826	0.5826	0.3519	0.1676
$\tau_{ms1}(s)$	$\tau_{ms2}(s)$	$U_{ms1}S_{ms1}(W^0C^{-1})$	$U_{ms2}S_{ms2}(W^0C^{-1})$	$c_{pfw}(J/kg.^0C)$	C_{tg}
0.3519	0.1676	1.7295×10^8	3.6312×10^8	5.4791×10^3	2.0481
$\frac{\partial T_{sat}}{\partial p_s}$ $(^0C/MPa)$	$h_{ss}(J/kg)$	$K_s(J/MPa)$	$T_{fw}(^0C)$	$m_s(kg)$	$m_w(kg)$
9.47	2.7656×10^6	8.1016×10^7	232.2	2.0518×10^3	1.8167×10^4
$d_w(kg/m^3)$	$d_s(kg/m^3)$	$V_w(m^3)$	$A_p(m^2)$	$l_w(m)$	$l(m)$
595.6684	100.9506	30.4988	3.566	8.5527	14.2524
$h_{spr}(J/kg)$	$h_w(J/kg)$	$h_{\bar{w}}(J/kg)$	$\nu_w(m^3/kg)$	$\nu_s(m^3/kg)$	J_p
1.336×10^6	1.6266×10^6	9.7209×10^5	1.7×10^{-3}	9.9×10^{-3}	5.4027
$V_1\vartheta_1(kg/^0C)$	$V_2\vartheta_2(kg/^0C)$	$V_3\vartheta_3(kg/^0C)$	$V_4\vartheta_4(kg/^0C)$	$V_5\vartheta_5(kg/^0C)$	$V_6\vartheta_6(kg/^0C)$
0.5991	0.1814	0.1814	1.3164	0.2752	2.776
$V_7\vartheta_7$ $(kg/^0C)$	$V_8\vartheta_8(kg/^0C)$	$V_9\vartheta_9(kg/^0C)$	$V_{10}\vartheta_{10}(kg/^0C)$	$K_{1p}(kg/kg.MPa)$	$K_{2p}(kg/m^3.MPa)$
0.6022	0.6022	0.2776	0.1927	-8.152×10^{-3}	4.708×10^{-3}
$K_{3p}(J/m^3.MPa)$	$K_{4p}(m^3/kg.MPa)$	F_{hp}	F_{ip}	F_{lp}	O_{rv}
-1.118×10^{-4}	4.708×10^{-3}	0.33	0	0.67	1.0
$\tau_{hp}(s)$	$\tau_{ip}(s)$	$\tau_{lp}(s)$	κ_{hp}	J_{tur}	$I_{tg}(kg.m^2)$
10.0	0.4	1.0	0.8	5.4040	1.99642×10^5
$\dot{m}_{sor}(kg/s)$	$\alpha_f(\Delta k/k/^0C)$	$\alpha_c(\Delta k/k/^0C)$	$\alpha_p(\Delta k/k/MPa)$	$\tau_1(s)$	$\tau_2(s)$
2.1642×10^3	-2.16×10^{-5}	-1.8×10^{-4}	1.5664×10^{-4}	5×10^{-8}	2×10^{-3}
$K_{lo}(mA)$	κ_{lo}	$\tau_3(s)$	$\tau_4(s)$	$K_{lr}(s)$	$\tau_{rtd}(s)$
1.95692	1.1067×10^{10}	1	1.01	47.065	8.2
$\tau_{co}(s)$	$m_{coh}(kg)$	$h_{cow}(J/kg)$	$h_{c\bar{o}w}(J/kg)$	$K_{rtd}(mA)$	$G(cent/step)$
7.0	41422.9	69.74	1036	10.667	9.679×10^{-1}
$K_{tg}(mA^{-1})$	ζ_{tg}	$\varpi_{tg}(rad/s)$	$C_{heat}(J/m.^0C)$	$R_{heat}(m.^0C/W)$	$K_{heat}(kW/mA)$
6.25	0.4933	14.6253	11.3	0.088	1000
$P(GWe)$	$T_{f0}(^0C)$	$T_{c10}(^0C)$	$T_{c20}(^0C)$	$T_{rxu0}(^0C)$	$T_{hot0}(^0C)$
1.2	626.66	312.13	327.30	327.30	327.30
$T_{sgi0}(^0C)$	$T_{sgu0}(^0C)$	$T_{cold0}(^0C)$	$T_{rxi0}(^0C)$	$T_{p10}(^0C)$	$T_{p20}(^0C)$
327.30	296.96	296.96	296.96	306.75	296.96
$T_{m10}(^0C)$	$T_{m20}(^0C)$	$T_{s0}(^0C)$	$p_{s0}(MPa)$	$p_{p0}(MPa)$	$l_{w0}(m)$
297.41	292.51	288.06	7.28	15.41	28.06
$T_{rtd10}(^0C)$	$T_{rtd20}(^0C)$	$i_{lo0}(mA)$	$i_{lr0}(mA)$	$i_{rtd0}(mA)$	$\omega_{tur0}(Hz)$
327.30	327.30	19.65	12	14.66	60

$$K_{1p} = \frac{\partial d_w}{\partial p_p}; K_{2p} = \frac{\partial d_s}{\partial p_p}; K_{3p} = \frac{\partial h_w}{\partial p_p}; K_{4p} = \frac{\partial \nu_s}{\partial p_p}; \quad (33)$$

F. Turbine Model

The amount of heat content of the steam flowing through the secondary side is obtained using the turbine model. The turbine converts the thermal energy into the mechanical energy. A typical turbine system is formed of four fundamentals blocks, high pressure (HP) turbine, moisture separator, re-heater, and low pressure (LP) turbine. The steam output of a SG is fed to the HP turbine where it gets expanded and a part of it is extracted and passed to the HP feed-water heater. The remaining part of the steam is passed to the moisture separator for water removal and then it is sent to the heater for super heating. The removed water is fed back to the HP feed-water system and the superheated steam is passed to the LP turbine. The LP turbine works similar to the HP turbine. The steam is then passed to the condenser. Finally, the turbine drives the generator system to produce corresponding electric output. The dynamical model containing equations of the HP turbine, re-heater, and LP turbine is given by [40]

$$\begin{aligned}
&\frac{d^2P_{hp}}{dt^2} + \left(\frac{O_{rv}+\tau_{ip}}{\tau_{hp}\tau_{ip}}\right)\frac{dP_{hp}}{dt} + \left(\frac{O_{rv}}{\tau_{hp}\tau_{ip}}\right)P_{hp} = \left(\frac{O_{rv}F_{hp}}{\tau_{hp}\tau_{ip}}\right)\bar{\dot{m}}_{so} \\
&\qquad + \left(\frac{(1+\kappa_{hp})F_{hp}}{\tau_{hp}}\right)\frac{d\bar{\dot{m}}_{so}}{dt} \\
&\frac{d^2P_{ip}}{dt^2} + \left(\frac{O_{rv}\tau_{hp}+\tau_{ip}}{\tau_{hp}\tau_{ip}}\right)\frac{dP_{ip}}{dt} + \left(\frac{O_{rv}}{\tau_{hp}\tau_{ip}}\right)P_{ip} = \left(\frac{O_{rv}F_{ip}}{\tau_{hp}\tau_{ip}}\right)\bar{\dot{m}}_{so} \\
&\frac{d^3P_{lp}}{dt^3} + \left(\frac{O_{rv}\tau_{hp}+\tau_{ip}}{\tau_{hp}\tau_{ip}} + \frac{1}{\tau_{lp}}\right)\frac{d^2P_{lp}}{dt^2} + \left(\frac{O_{rv}(\tau_{lp}+\tau_{hp})+\tau_{ip}}{\tau_{hp}\tau_{ip}\tau_{lp}}\right) \\
&\qquad \frac{dP_{lp}}{dt} + \left(\frac{O_{rv}}{\tau_{hp}\tau_{ip}\tau_{lp}}\right)P_{lp} = O_{rv}F_{lp}\bar{\dot{m}}_{so}
\end{aligned} \quad (34)$$

where the steam flow in turbine is $\bar{\dot{m}}_{so} = \dot{m}_{so}/\dot{m}_{sor}$, $\dot{m}_{sor}$ is the rated steam mass flow rate. Therefore, the mechanical output of turbine is given by

$$P_{tur} = P_{hp} + P_{ip} + P_{lp}. \tag{35}$$

The turbine-generator model consists of a turbine speed system which produces variation in turbine speed in accordance with the difference in the demand power and turbine output. The turbine-generator inertia equation relating turbine speed with the power can be written as

$$\frac{d\omega_{tur}}{dt} = \frac{P_{tur} - P_{dem}}{(2\pi)^2 J_{tur}\omega_{tur} I_{tg}} \tag{36}$$

G. Condenser Model

The turbine exhaust flow enters the system at the condenser, where the water part of the flow falls into the hot-well region and the vapour part condenses on the outer surface of metal tubes. The heat transfer between the vapour and the circulating water is associated with a time delay. The condenser remains in a thermal equilibrium of steam and water. Thus, using the mass and energy conservation at each phase, gives the rate of change of the enthalpy at the outlet:

$$\frac{dh_{wo}}{dt} = \frac{(\dot{m}_{coh} + \dot{m}_{cow})(h_{cow} - h_{wo})}{m_{coh}} \tag{37}$$

and the mass balance relations are

$$\dot{m}_{coh} = \dot{m}_{lp} - \dot{m}_{cow} \tag{38}$$

$$\dot{m}_{cow} = \dot{m}_{lp}\frac{(h_{lp} - h_{cow})}{h_{c\bar{o}w}} \tag{39}$$

$$\frac{d\dot{m}_{cos}}{dt} = \frac{\dot{m}_{cow} - \dot{m}_{cos}}{\tau_{co}}. \tag{40}$$

H. Reactivity Model

The reactivity model consists of internal reactivity feedbacks due to variation in fuel and coolant temperatures and primary coolant system pressure and external reactivity devices. The total reactivity is given by

$$\rho_t = \rho_{rod} + \rho_f + \rho_{c1} + \rho_{c2} + \rho_p, \tag{41}$$

It can be expanded as,

$$\rho_t = \rho_{rod} + \alpha_f T_f + \alpha_c T_{c1} + \alpha_c T_{c2} + \alpha_p p_p. \tag{42}$$

III. Sensors & Actuators

A. Sensors

1) Ex-core Detectors and Amplifiers: The global power in a reactor can be monitored using ex-core detectors and their associated amplifiers [2]. The ex-core detectors produces a current signal proportional to the total power. These detectors are placed outside the core and thus require a logarithmic amplifier to amplify the sensed current signal [41]. This amplification stage can be represented by

$$\tau_1\tau_2\frac{d^2 i_{lo}}{dt^2} + (\tau_1 + \tau_2)\frac{di_{lo}}{dt} + i_{lo} = K_{lo}\log_{10}(\kappa_{lo}P_n), \tag{43}$$

A logarithmic rate current signal is given by [2], [41]

$$\tau_3\tau_4\frac{d^2 i_{lr}}{dt^2} + (\tau_3 + \tau_4)\frac{di_{lr}}{dt} + i_{lr} - 12 = K_{lr}\frac{di_{lo}}{dt}. \tag{44}$$

2) Resistance Temperature Detector: Resistance temperature detectors (RTD) are used to measure primary coolant temperature. RTDs are used to sense coolant temperature and its transmitter at the inlet and outlet [2], [41]. It is given by

$$\frac{dT_{rtd1}}{dt} = \frac{1}{\tau_{rtd}}(-T_{rtd1} + 2T_{c1} - T_{rxi}) \tag{45}$$

$$\frac{dT_{rtd2}}{dt} = \frac{1}{\tau_{rtd}}(-T_{rtd2} + 2T_{c2} - T_{rxu}) \tag{46}$$

A proportional current signal can be obtained from the sensed RTD signals as

$$i_{rtd} = K_{rtd}\frac{(T_{rtd} - T_{rxi0})}{(T_{rxu0} - T_{rxi0})} + 4 \;\; mA \tag{47}$$

where $T_{rtd} = (T_{rtd1} + T_{rtd2})/2$ is the average RTD temperature.

B. Actuators

1) Control Rod: The change in reactivity due to control rod movement is related to the speed of rod movement in terms of number of steps per minute (spm). It is given by

$$\frac{d\rho_{rod}}{dt} = Gv_{rod} \tag{48}$$

where the control rod is assumed to have uniform worth distribution along its length.

2) Turbine-Governor Valve: The turbine-governor control valve coefficient can be adjusted using the input signal to the valve. The control valve dynamics can be described by a second order differential equation:

$$\frac{d^2 C_{tg}}{dt^2} + 2\zeta_{tg}\varpi_{tg}\frac{dC_{tg}}{dt} + \varpi_{tg}^2 C_{tg} = \varpi_{tg}^2 K_{tg}u_{tg} \tag{49}$$

The input signal to the valve is actuated either when there is a steam pressure difference from the set-point as shown in Fig. 6, or if there is mismatch in the turbine speed from the reference speed as shown in Fig. 9.

3) Pressurizer Heater: The pressurizer heater system relates input current to the heat output. A simple heater system can be given by a first order differential equation as

$$C_{heat}\frac{dQ_{heat}}{dt} + \frac{Q_{heat}}{R_{heat}} = K_{heat}i_{heat} \tag{50}$$

IV. System Analysis

The overall nonlinear system given by (1–50) can be linearised to analyse the linear system properties. It can be represented in standard state-space form as,

$$\begin{aligned}\frac{dx}{dt} &= Ax(t) + Bu(t),\\ y(t) &= Cx(t) + Du(t)\end{aligned} \tag{51}$$

where $A \in \mathbb{R}^{n\times n}$, $B \in \mathbb{R}^{n\times m}$, $C \in \mathbb{R}^{l\times n}$, and $D \in \mathbb{R}^{l\times m}$ are system matrices. $u(t) \in \mathbb{R}^m$, $y(t) \in \mathbb{R}^l$, and $x(t) \in \mathbb{R}^n$

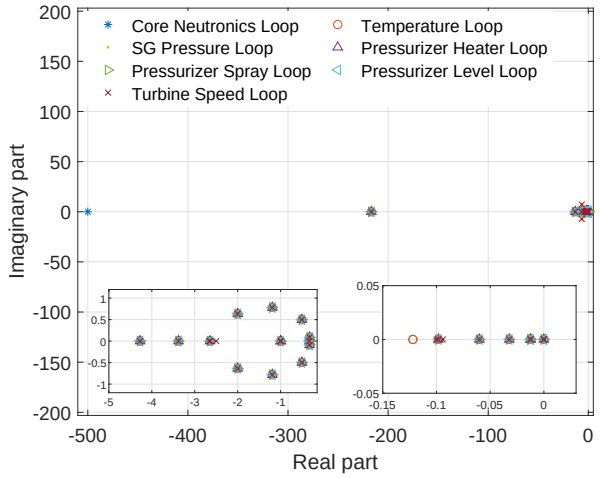

Fig. 2: Eigenvalues plot of the system matrix.

represent control input, system output, and state, respectively. The value of typical parameters employed in the model are listed in Table I [1], [2], [7], [8], [12]–[16], [40].

A. Stability

A system is said to be bounded-input bounded-output stable if every bounded input $u(t)$ excites a bounded output $y(t)$. Moreover, the system $\frac{dx}{dt} = Ax(t)$ is marginally stable or stable in the sense of Lyapunov if every finite initial state $x(0) = x_0$ excites a bounded state response $x(t), t > 0$. Asymptotic stability implies that every finite initial state excites a bounded state response which, in addition, will approach 0 asymptotically [42]. The stability properties of the linear system depend on the position of the eigenvalues of the system matrix A. For instance, the system $\frac{dx}{dt} = Ax(t)$ is asymptotically stable if and only if all eigenvalues of A have negative real parts. The same system is said to be marginally stable if the eigenvalues of A have zero or negative real part, and those with zero real parts are simple roots of the characteristic polynomial of A. It is known that a nuclear power plant, in the absence of any reactivity feedback effects, is not asymptotically stable. Internal reactivity feedbacks due to temperature variations further affect the stability of the system [43]. Fig. 2 depicts the plot of eigenvalues of the linear system matrices. None of the eigenvalues of the systems are found to be have a positive real part. However, the models exhibit multiple eigenvalues at the origin, which makes the linearised models asymptotically unstable. The single input single output models formed in loops such as core neutronics, temperature, pressurizer level, and turbine speed each contain two eigenvalues each at the origin whereas the model in steam generator pressure, pressurizer heater, and pressurizer spray loop each contain one eigenvalue at the origin.

B. Controllability

A linear system is said to be controllable if and only if the system states can be changed by changing the system input. A linear system with order n is said to be controllable if and only if the controllability matrix ζ has rank n, where $\zeta = \begin{bmatrix} B & AB & \cdots & A^{n-1}B \end{bmatrix}$. Designing a controller to stabilize an unstable system such as a nuclear power plant and to achieve any specified transient response characteristics may not be possible if the system is uncontrollable. It is noticed that the proposed nuclear power plant model exhibits full controllability which governs the existence of a complete solution to the linear control system design problem.

C. Observability

A linear system is said to be observable if and only if the value of the initial states can be determined from the system output observed over a finite time interval. A linear system with order n is said to be observable if and only if the observability matrix ξ has rank n, where $\xi = \begin{bmatrix} C^T & C^T A & \cdots & C^T A^{n-1} \end{bmatrix}$. The concept of observability thus helps in solving the problem of reconstructing unmeasured state variables from the measured variables. This concept plays a significant role in control system design since the information of all the values of the state variables, which is essential for implementing a state feedback controller, is normally not available. For instance, precursors' concentrations are not measurable in an nuclear power plant. It is noticed that the proposed nuclear power plant model is observable.

D. Model Validation

The task of system modelling is incomplete without model validation. The simulated model output is compared with the real measured output from the plant to check the validity of the model. The accuracy of the model can be assessed by observing the percentage deviation (E) of the model output (Y_{model}) from the plant output (Y_{plant}) as

$$E = \frac{Y_{plant} - Y_{model}}{Y_{model}} \times 100\% \tag{52}$$

The proposed model is validated using two datasets obtained from the H. B. Robinson nuclear power plant as reported in [12]. The perturbation in the control rod input signal is shown in Fig. 3a and the corresponding normalized reactor power output is shown in Fig. 3b. The percentage deviation between the reactor power output of the plant and that of the model is shown in Fig. 3c. It can be noticed that the model response accurately tracks the trends in the power response of the plant. The perturbation in steam flow input is shown in Fig. 4a and the corresponding normalized steam pressure output is shown in Fig. 4b. The deviation between plant and model steam pressure outputs is shown in Fig. 4c. The model output is able to closely track the steam pressure response of the plant. The correlation between the plant response and the model response is very good in both cases.

E. Limitations

In this section the main limitations of the presented model are discussed. The integrated model of the nuclear power plant does not represent the spatial behaviour of the core neutronics. Hence, this model is not suitable to study the effects that occur

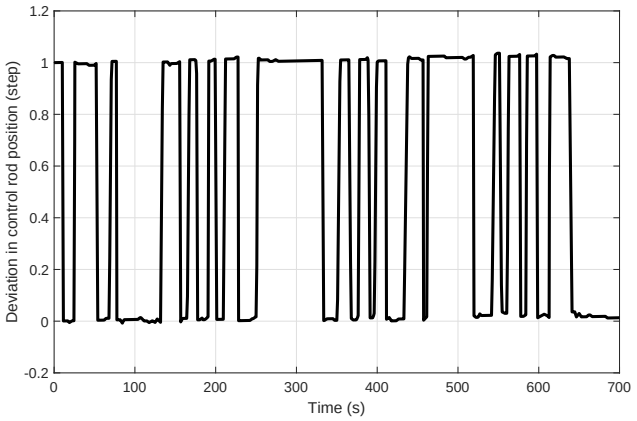

(a) Control rod position.

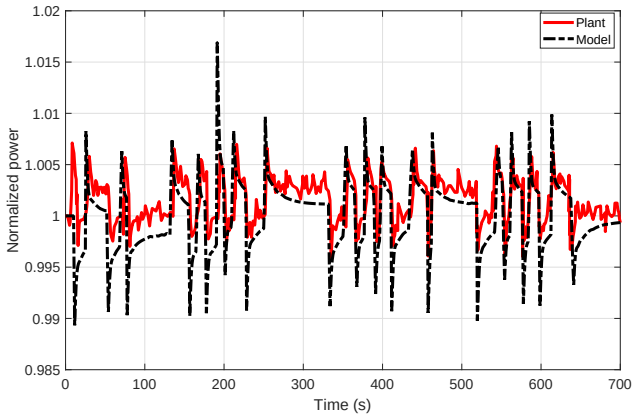

(b) Reactor power.

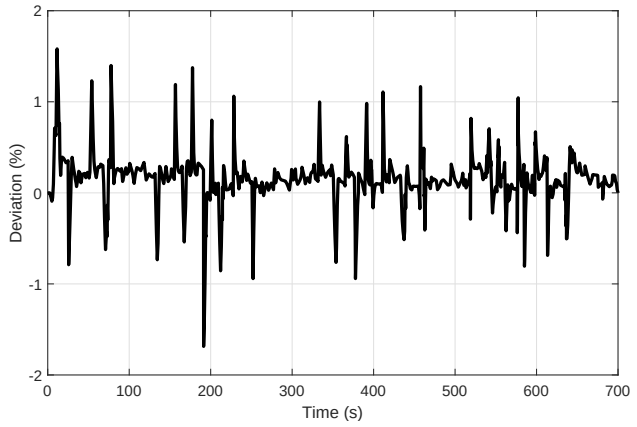

(c) Deviation between plant and model response.

Fig. 3: Comparison of plant and model responses.

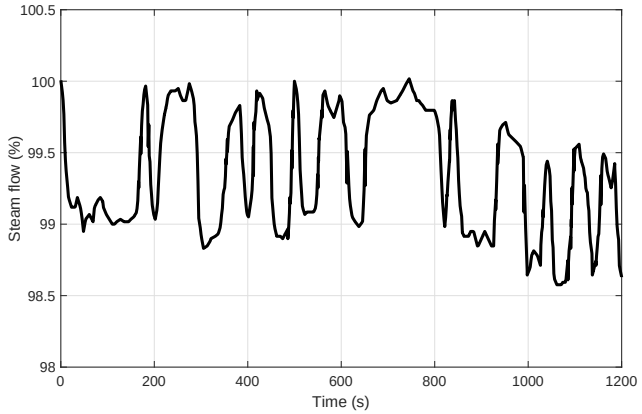

(a) Steam flow.

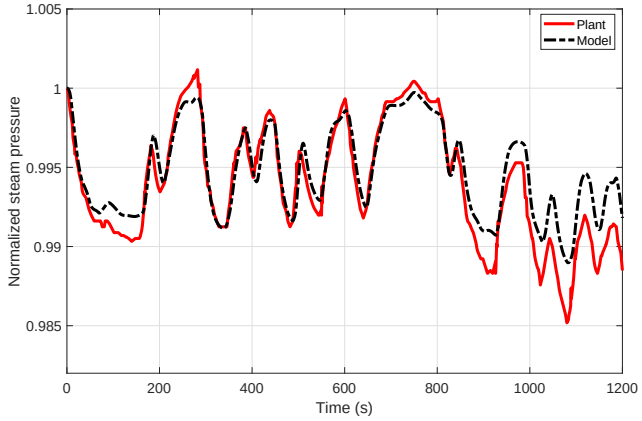

(b) Steam pressure.

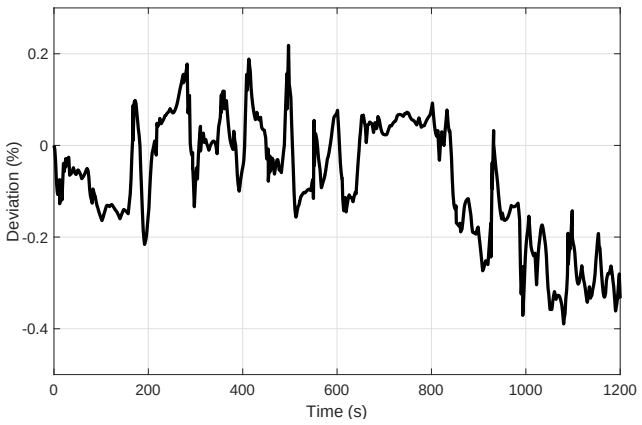

(c) Deviation between plant and model response.

Fig. 4: Comparison of plant and model responses.

due to spatial phenomena, such as flux tilt or local power peaking. The model does not consider reactivity feedbacks due to xenon poisoning, and the dynamics of xenon oscillations are neglected. Further, the model does not consider the reactivity control due to boron, which is used for long-term control of core reactivity.

V. Design of Nuclear Power Plant Control Loops

In this section different control loops are designed. The low-level PI control scheme is also formulated for each loop. The definition of input and output signals for every single-input single-output control loop and the value of tuned controllers gains are given in Table II.

A. Reactor Power Control Loop

The reactor power can be controlled directly using neutronic power, indirectly through average coolant temperature, or through a combination of both power and temperature. Both controllers compare the measured values with the reference values based on turbine power, which is related to the turbine impulse pressure. In this section three different configurations in the reactor power control loop are studied.

TABLE II: Controller tuning parameters for different configurations

Configuration			PID		LQG			
Control Loop	Input	Output	K_P	K_I	Q	R	Ξ	Θ
Core Neutronics	v_{rod}	i_{lo}	3.087×10^{-2}	3.947×10^{-3}	$1 \times 10^{-3} I_n$	1×10^{5}	$5 \times 10^{0} I_n$	1
Temperature	v_{rod}	i_{rtd}	1.930×10^{-3}	1.006×10^{-5}	$1 \times 10^{-3} I_n$	1×10^{5}	$1 \times 10^{0} I_n$	1
SG Pressure	u_{tg}	p_s	5.368×10^{-1}	1.169×10^{-1}	$5 \times 10^{-3} I_n$	1×10^{-3}	$5 \times 10^{-5} I_n$	1
Pressurizer (Heater)	i_{heat}	p_p	4.092×10^{3}	2.861×10^{2}	$1 \times 10^{-3} I_n$	1×10^{-3}	$1 \times 10^{-2} I_n$	1
Pressurizer (Spray)	$\dot{m}_{spr}$	p_p	2.935×10^{5}	1.695×10^{5}	$1 \times 10^{6} I_n$	1×10^{-4}	$5 \times 10^{-5} I_n$	1
Pressurizer Level	$\dot{m}_{sur}$	l_w	1.275×10^{3}	7.366×10^{2}	$1 \times 10^{6} I_n$	1×10^{-5}	$5 \times 10^{0} I_n$	1
Turbine Speed	u_{tg}	ω_{tur}	6.430×10^{2}	8.426×10^{0}	$1 \times 10^{3} I_n$	1×10^{-2}	$5 \times 10^{-3} I_n$	1

1) Core Neutronics Control Loop: This loop directly controls the reactor power using ex-core detector current output of the amplifier. The error signal generated between the reference and measured value of current is fed-back to the controller acting in the power loop to minimize the effect of disturbances. In the presence of a disturbance, the controller acts to minimize its effect by regulating the control signal using feedback signal. The control action is obtained by a PI controller which takes the mismatch between the set-point and actual value of the measured current output of amplifier. The control signal is given by

$$v_{rod} = \left(K_{P,lo} + \frac{K_{I,lo}}{s} \right) (i_{lo0} - i_{lo}) \tag{53}$$

where $K_{P,lo}(spm/mA)$ and $K_{I,lo}(spm/s.mA)$ are proportional and integral gains, respectively.

2) Temperature Control Loop: In this configuration the reactor power is controlled indirectly by controlling the average coolant temperature. The current measured by RTDs is fed-back to the comparator. The error signal is then applied to the controller acting in the temperature control loop to derive the control signal. The control signal obtained by a PI controller is given by

$$v_{rod} = \left(K_{P,rtd} + \frac{K_{I,rtd}}{s} \right) (i_{rtd0} - i_{rtd}) \tag{54}$$

where $K_{P,rtd}(spm/mA)$ and $K_{I,rtd}(spm/s.mA)$ are proportional and integral gains, respectively.

3) Combined Neutronics and Temperature Control Loop: A combination of core neutronics power feedback and temperature feedback are employed to design the overall reactor power control loop. The control signal is derived from the combination of current sensed by the ex-core detector and the RTD. The overall PI controller output is a summation of the PI controller control signal from power feedback loop and the PI controller control signal from temperature feedback loop. The control signal is given by

$$v_{rod} = \left(\tilde{K}_{P,lo} + \frac{\tilde{K}_{I,lo}}{s} \right) (i_{lo0} - i_{lo}) + \left(\tilde{K}_{P,rtd} + \frac{\tilde{K}_{I,rtd}}{s} \right) (i_{rtd0} - i_{rtd}) \tag{55}$$

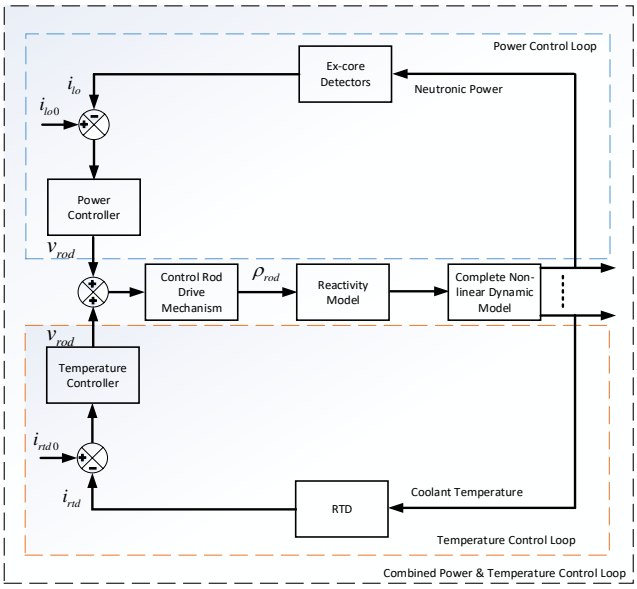

Fig. 5: Reactor power control loop.

where $\tilde{K}$ represent the retuned gains. All the three above-mentioned configurations are shown in Fig. 5. A typical control rod drive mechanism given by Westinghouse has been adopted [38]. The control rod drive mechanism limits the maximum and minimum rod steps per minute based on the temperature error. The rod speed program converts the temperature error to rod motion. The maximum rod speed is limited to 72 spm and a deadband of $\pm 0.55^0 C$ is considered.

B. Steam Generator Pressure Control Loop

Control of SG pressure is achieved by adjusting the turbine-governor valve opening. The valve opening is controlled by an input signal to the control valve through a valve system. A controller is designed to minimize the effect of disturbances in the SG pressure loop. The steam pressure control loop configurations is shown in Fig. 6. In the presence of a feedback action from SG pressure loop, the feedback pressure signal is compared with the reference value of pressure to minimize the effect of a disturbance. The steam pressure output is measured and fed-back to the comparator. The generated error signal is fed-back to the controller acting in the steam pressure loop to

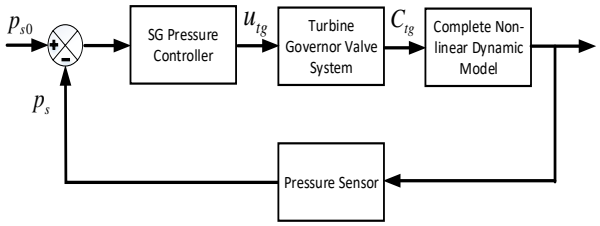

Fig. 6: Steam generator pressure control loop.

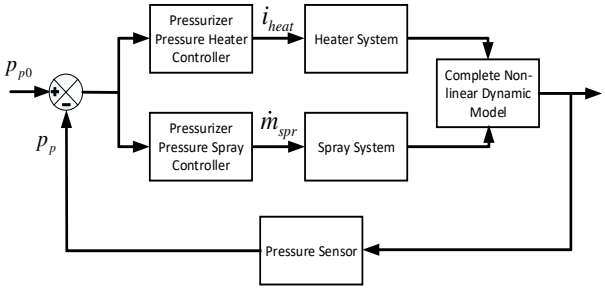

Fig. 7: Pressurizer pressure control loop.

minimize the effect of a disturbance. The control signal output obtained by a PI controller is given by

$$u_{tg} = \left(K_{P,s} + \frac{K_{I,s}}{s}\right)(p_{s0} - p_s) \tag{56}$$

where $K_{P,s}(1/MPa)$ and $K_{I,s}(1/s.MPa)$ are proportional and integral gains, respectively.

C. Pressurizer Control Loop

The pressurizer control system consists of pressure and level control loops. The purpose of a level control system in the pressurizer is to maintain the water level for the reactor core coolant system. The pressure control system controls the coolant pressure and maintains it within permissible limit.

1) Pressurizer Pressure Control Loop: Control of the primary coolant system pressure is achieved by bank of heaters, spray flow rate, power operated relief valves, and safety valves. In this study the pressure control is achieved either by a bank of heaters or by maintaining the spray flow rate. Both of them compensate for steady-state heat losses from the pressurizer and also regulate the pressure under normal operating conditions. The pressurizer pressure program selects the heater or the spray system based on the pressure deviation. In a Westinghouse-type PWR [38], the heater or spray flow systems is actuated if the pressure changes from the reference set-point of 15.41 MPa. The heater system works between 15.30 MPa and 15.51 MPa whereas the spray flow rate system is actuated between 15.58 MPa and 15.92 MPa. A deadband exists between 15.51 MPa and 15.58 MPa. The model used in this work includes only the normally operating heater. The pressurizer pressure control loop configuration is shown in Fig. 7. The pressure signal from the model output is fed back

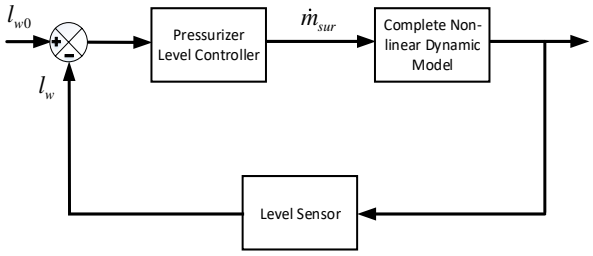

Fig. 8: Pressurizer level control loop.

to the comparator to produce an error signal, which in turn goes either into the heater control system and into the spray flow rate controller to minimize the effect of the disturbance. It should be noted that only one controller acts at a time. The control signal output obtained from the heater PI control system is given by

$$i_{heat} = \left(K_{P,heat} + \frac{K_{I,heat}}{s}\right)(p_{p0} - p_p)\,\theta\,(p_{p0} - p_p) \tag{57}$$

and the control signal from the spray PI controller system is given by

$$\dot{m}_{spr} = \left(K_{P,spr} + \frac{K_{I,spr}}{s}\right)(p_{p0} - p_p)\,\theta\,(p_p - p_{p0}) \tag{58}$$

where $K_{P,heat}(mA/MPa)$ and $K_{P,spr}(kg/s.MPa)$ are proportional gains and $K_{I,heat}(mA/s.MPa)$ and $K_{P,spr}(kg/s^2.MPa)$ are integral gains, respectively. $\theta\,(\cdot)$ represent the heaviside step function.

2) Pressurizer Level Control Loop: During transients the water level in the pressurizer changes due to expansion or contraction in the coolant as the average temperature of the coolant increases or decreases. The pressurizer level is maintained by varying the charging flow using charging flow control valves in the discharge header of the charging pumps [44]. The pressurizer level control loop configuration is shown in Fig. 8. An unchanging pressurizer level indicates that the charging flow into the reactor coolant system and the let-down flow from the reactor coolant system is constant. If a difference exists, then the charging flow is varied by varying the position of charging flow control valves. Here, the charging flow control is provided by a PI controller. In case of pressurizer level control, the control signal is calculated based on the level difference in water inventory. The control signal is given by

$$\dot{m}_{sur} = \left(K_{P,sur} + \frac{K_{I,sur}}{s}\right)(l_{w0} - l_w) \tag{59}$$

where $K_{P,sur}(kg/s.m)$ and $K_{P,sur}(kg/s^2.m)$ are proportional and integral gains, respectively.

D. Turbine Speed Control Loop

The generator coupled to the turbine produces electricity at a constant frequency. The frequency stays constant if the turbine shaft speed remains constant. Initially, the turbine speed is set according to the design frequency of the generator. In the absence of a turbine speed control system, the turbine speed

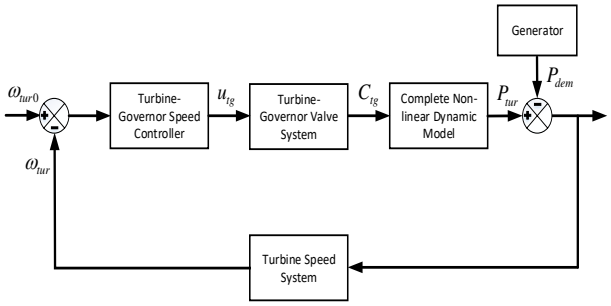

Fig. 9: Turbine speed control loop.

will vary with the variation in demand. The turbine speed control loop configuration is shown in Fig. 9. In a typical turbine speed control system, the speed can be regulated by controlling the steam flow to the turbine through a turbine-governor valve. Any changes at the valve position will be proportional to the turbine output torque which ultimately regulates the speed. The control signal from the PI controller of the turbine speed control loop is given by

$$u_{tg} = \left(K_{P,tur} + \frac{K_{I,tur}}{s}\right)(\omega_{tur0} - \omega_{tur}) \tag{60}$$

where $K_{P,tur}(s)$ and $K_{P,tur}$ are proportional and integral gain, respectively.

VI. Linear Quadratic Gaussian Control Design

The design of LQG controller involves design of a state estimator using Kalman filter and the design of an optimal state feedback control using LQR.

1) Kalman Filter: The Kalman filter estimation problem is to find an optimal state estimate $\hat{x}(t)$ such that the following error covariance is minimized:

$$J_1 = \lim_{t\to\infty} E\left\{(x-\hat{x})(x-\hat{x})^T\right\} \tag{61}$$

The Kalman filtering problem is estimated by computing the Kalman gain K_f given by

$$K_f = P_f C^T \Theta^{-1} \tag{62}$$

where P_f is a symmetric positive semidefinite matrix and can be computed using the solution of following Algebraic Riccati Equation (ARE) as

$$AP_f + P_f A^T + \Gamma\Xi\Gamma^T - P_f C^T \Theta^{-1} C P_f = 0 \tag{63}$$

where $\Gamma \in \mathbb{R}^{n\times m}$ is disturbance input matrix. $E\left(\omega(t)\omega(t)^T\right) = \Xi$ and $E\left(\upsilon(t)\upsilon(t)^T\right) = \Theta$ are covariance of process noise ($\omega(t)$) and measurement noise ($\upsilon(t)$), respectively. Thus, the estimated states $\dot{\hat{x}}(t)$ are given by,

$$\dot{\hat{x}}(t) = A\hat{x}(t) + Bu(t) + K_f(y(t) - C\hat{x}(t)) \tag{64}$$

2) Linear Quadratic Regulator: The Linear Quadratic Regulator (LQR) design computes an optimal control input by minimizing the following cost function

$$J_2 = \int_0^\infty \left(\hat{x}^T Q\hat{x} + u^T Ru\right) dt \tag{65}$$

where Q and R are positive semidefinite and positive definite weighing matrices, respectively. The cost function can be minimized by finding the solution of the following ARE to calculate optimal regulator feedback gain. The ARE is given by

$$A^T P_c + P_c A + Q - P_c B R^{-1} B^T P_c = 0 \tag{66}$$

where P_c is a symmetric positive semidefinite matrix. The optimal regulator feedback gain is computed as

$$K_c = R^{-1} B^T P_c \tag{67}$$

The optimal state feedback control law is implemented using the estimated states. The control law for error dynamics is then given by

$$u(t) = -R^{-1} B^T P_c \hat{x}(t) \tag{68}$$

VII. Dynamic Model Response

This section presents the dynamic response of the non-linear model to different perturbations in the input variables. Initially, the plant is assumed to be operating at a steady state. For each case, the input variable under investigation is perturbed at $t = 20$s and the corresponding variation in plant behaviour is noted, while other variables are kept constant.

A. Variation in Control Rod Movement

An instantaneous perturbation is applied in the control rod movement which produces a step variation in the reactivity. This increases the fission rate by reducing the neutron absorption inside the core and thus causing a prompt jump in the reactor power. Due to significant reactivity feedback from fuel and coolant temperatures, the power decreases and stabilises at a new steady state value (Fig. 10a). Consequently, this leads to a rise in the fuel temperature (Fig. 10b), which increases the heat transfer to the coolant and thereby raises the coolant temperatures (Fig. 10c–10d). The increase in the temperature at the hot-leg (Fig. 10e) causes an increment in the heat transfer from SG inlet plenum to primary side and then subsequently to the secondary side and to the cold-leg (Fig. 10f). The variation in the temperatures of PCL 1 and 2 and MTL 1 and 2 are shown in Figs. 10g–11b, respectively. The rise in the temperature of SCL (Figs. 11c) increases the SG pressure (Fig. 11d). The increase in the temperature of the primary side leads to an expansion of the coolant volume, which leads to a surge flow into the pressurizer thereby increasing the pressure (Fig. 11e). The variation in mass flow rate raises the turbine output (Fig. 11f). The % variation in reactivity is shown in Fig. 11h. The reactivity feedback from fuel temperature, coolant temperature, and primary coolant pressure can be plotted using Figs. 10b, 10c, and 11e, respectively. The total change in reactivity is shown in Fig. 11g.

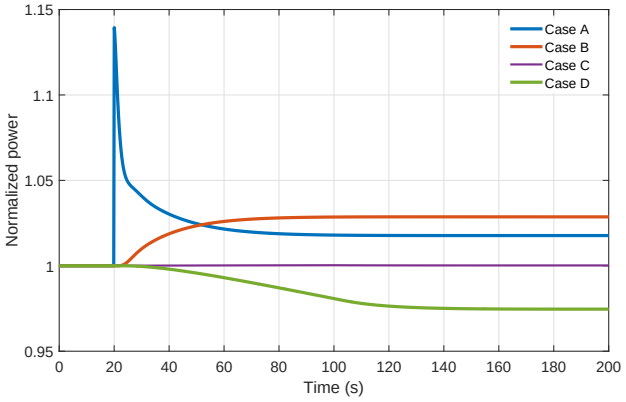

(a) Reactor power.

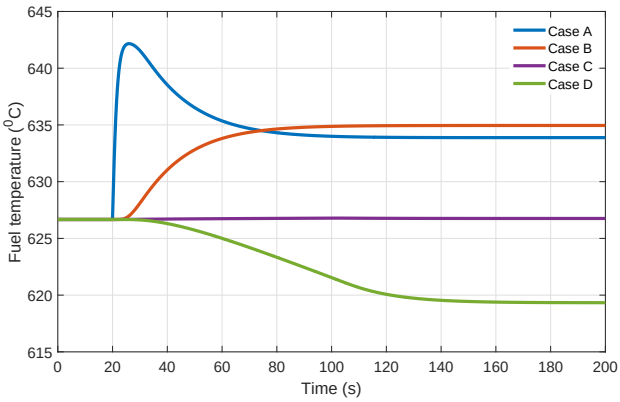

(b) Fuel temperature.

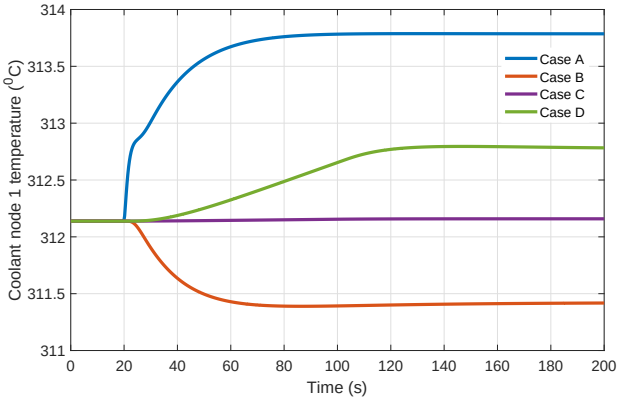

(c) Coolant node 1 temperature.

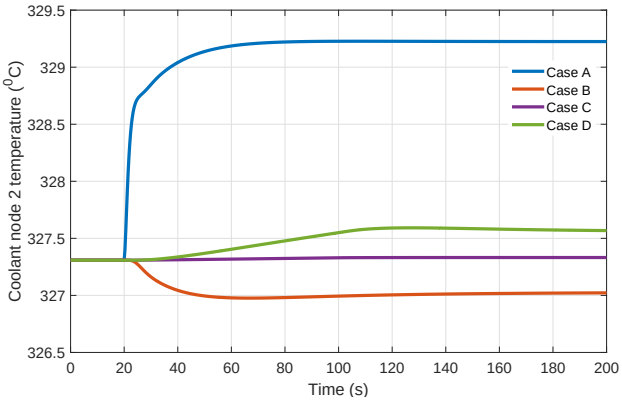

(d) Coolant node 2 temperature.

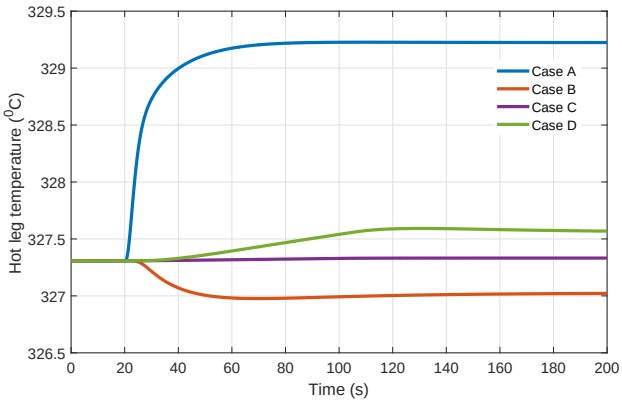

(e) Hot-leg temperature.

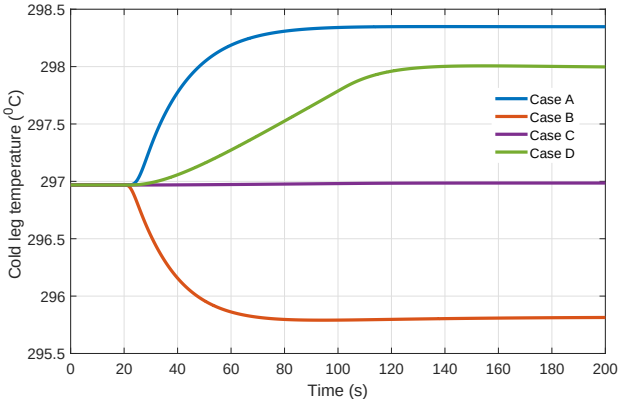

(f) Cool-leg temperature.

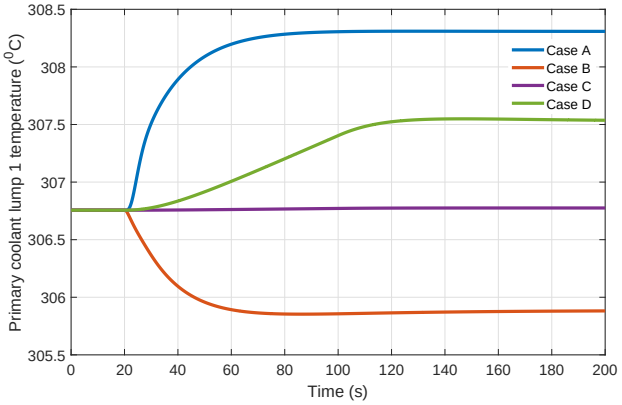

(g) PCL 1 temperature.

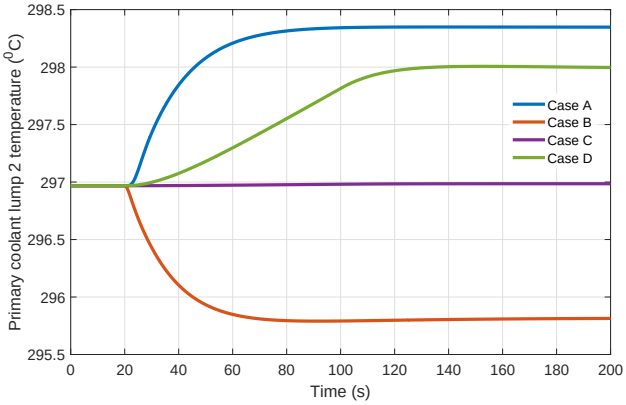

(h) PCL 2 temperature.

Fig. 10: Variation in different variables for perturbations in the input.

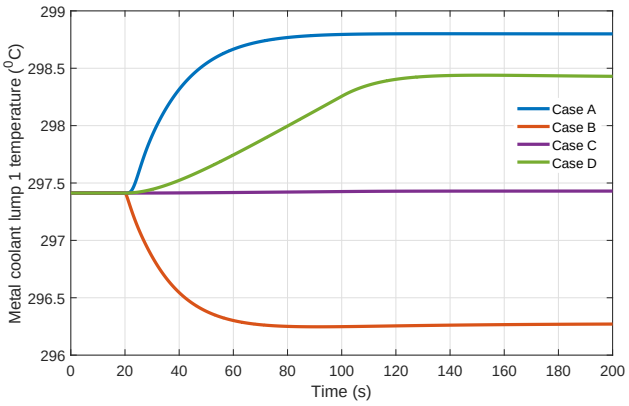

(a) MTL 1 temperature.

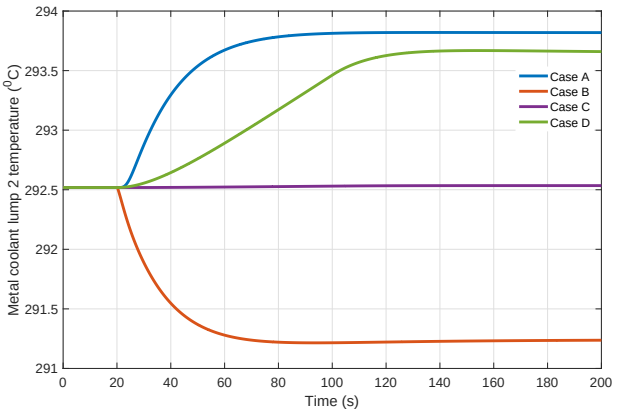

(b) MTL 2 temperature.

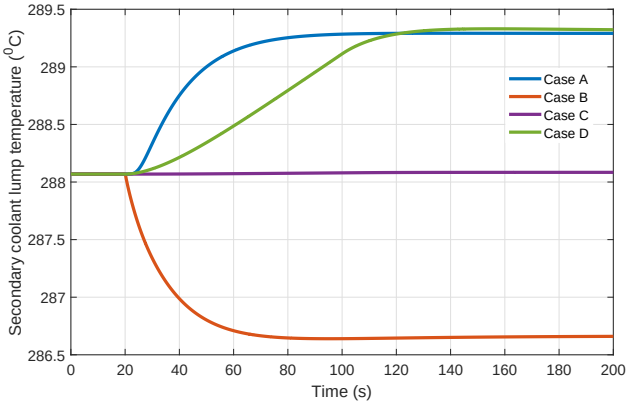

(c) SCL temperature.

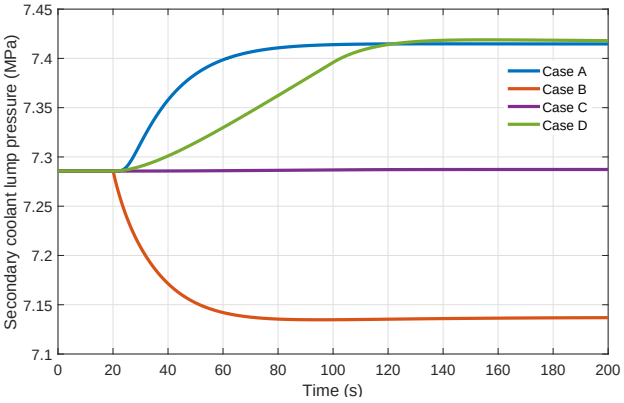

(d) Steam generator pressure.

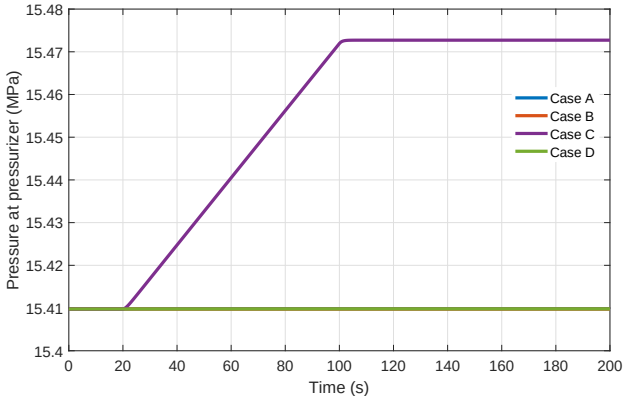

(e) Pressurizer pressure.

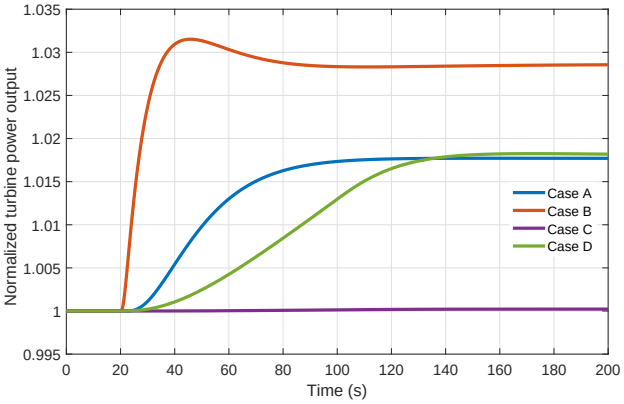

(f) Turbine output.

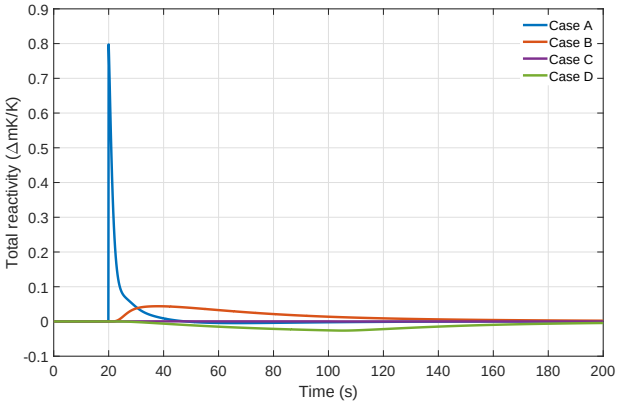

(g) Total reactivity.

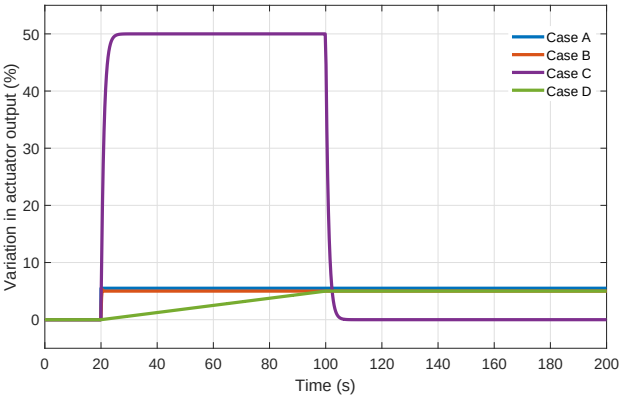

(h) Actuator outputs.

Fig. 11: Variation in different variables for perturbations in the input.

B. Change in Valve Coefficient

A step change is applied in the input signal to the turbine-governor valve which increases the valve coefficient. This causes a decrement in the steam pressure (Fig. 11d) and thus an increment in the brief production of steam demand. This leads to an increase in the heat transfer from the primary side to the secondary thereby decreasing temperatures of the PCL 1 and 2 (Figs. 10g–10h) and MTL 1 and 2 (Figs. 11a–11b), respectively. Due to a decrease in the temperature of SCL (Fig. 11c), a corresponding reduction in SG pressure is noted (Fig. 11d). The reduction in the primary coolant temperatures lead to a decrement in the pressurizer pressure until a new equilibrium is established due to reduction in the coolant volume in the primary loop (Fig. 11e). The reduction in coolant temperatures (Figs. 10c–10d), hot-leg (Fig. 10e) and cold-leg (Fig. 10f) are also observed. This induces a positive reactivity into the system, thereby leading to a gradual increase in the reactor power (Fig. 10a) and a corresponding increase in fuel temperature (Fig. 10b). The variation in mass flow rate raises the turbine output (Fig. 11f). The total change in reactivity is plotted in Fig. 11g. The % variation in valve coefficient is shown in Fig. 11h.

C. Variation in Heater Input

A step change is applied in the current input to the heater from $t = 20$s to $t = 100$s, which produces a corresponding variation in the heater output. A very slight change in the reactor neutronic power (Fig. 10a) is observed due to positive reactivity feedback. Consequently, temperatures of fuel (Fig. 10b), coolant node 1 and 2 (Figs. 10c–10d), hot-leg (Fig. 10e) and cold-leg (Fig. 10f) are also slightly increased. It causes a slight increment in the heat transfer from SG inlet plenum to PCL 1 and 2 (Figs. 10g–10h) and to MTL 1 and 2 (Figs. 11a–11b). Subsequently, the temperature of SCL (Fig. 11c) and the pressure of SG (Fig. 11d) are also increased. Due to the heat addition, more heat is transferred to the the pressurizer which leads to a rise in the pressurizer pressure until the heaters are turned off (Fig. 11e). The slightly increased turbine output can be seen in Fig. 11f. The % variation in pressurizer heater output is shown in Fig. 11h. After the heater input is turned off, the reactivity feedback mechanisms bring the system reactivity back to its initial value. The total change in reactivity is plotted in Fig. 11g. It can be noted that the reactor remains at a slightly elevated temperature and pressure compared to the initial equilibrium condition. However, the overall effect does not have a significant impact on the reactor state.

D. Change in Feed-Water Temperature

A ramp variation is applied in the feed-water inlet temperature from $t = 20$s to $t = 100$s which decreases the heat transfer from primary to secondary side and causes the secondary side temperature to rise. The variation in temperatures of PCL 1 and 2 and MTL 1 and 2 are plotted in Figs. 10g–11b, respectively. It leads to an increment in the primary coolant temperature at the SG outlet as well as at the reactor outlet. The temperatures of coolant nodes 1 and 2 (Figs. 10c–10d), hot-leg (Fig. 10e), and cold-leg (Fig. 10f) are plotted. The reactivity starts decreasing due to feedback and reductions in both reactor neutronic power (Fig. 10a) and fuel temperature (Fig. 10b) are observed. The overall increment in the temperature of the coolant leads to an increase in the temperature of SCL (Fig. 11c) and also of the pressure of SG (Fig. 11d). The pressure at the pressurizer is plotted in Fig. 11e. The increment in mass flow rate leads to an increment in the turbine output as shown in Fig. 11f. The total change in reactivity is shown in Fig. 11g. The % variation in feed-water temperature is shown in Fig. 11h.

VIII. Nuclear power plant Control Loop Response

In this section, the PI and LQG controllers are tested to analyse the closed-loop performance of the plant.

A. Reactor Power Control Loop

A step change in reactivity is applied as a disturbance at $t = 20$s. During open-loop, the step change in reactivity causes a sudden increment in power and in the ex-core detector current and shifts their steady-state values. In the presence of feedback, the controller acts to reject the disturbance and bring back the current to the initial value. The control response of PI and LQG controllers is plotted in Fig. 12. Both controllers are able to reject the disturbance. The PI controller quickly acts to reject the disturbance however with peak overshoot and undershoot in both ex-core detector current and RTD current. For core neutronics loop, the response of ex-core detector current and the external reactivity injected by control rods to handle the disturbance are plotted in Figs. 12a and 12b, respectively. For temperature loop, the response of RTD current and the external reactivity are plotted in Figs. 12c and 12d, respectively. In both cases, the LQG controller rejects the disturbance better than the PI controller and with lesser control efforts.

B. Steam Generator Pressure Control Loop

A step change in the turbine-governor valve coefficient is applied as a disturbance at $t = 20$s. In open-loop, the SG pressure decreases due to increase in valve coefficient and shifts the pressure to a lower steady state value. Whereas, in closed-loop, the controller acts effectively to minimize the effect of disturbance and brings back the steam pressure to its initial steady state. The performance of the PI and LQG controllers in rejecting the disturbance is shown in Fig. 13a and 13b. It is observed that the both controllers are able to maintain the steam pressure at its set-point. The PI controller produces a large overshoot before settling to its initial set-point. The LQG controller rejects the disturbance with lesser variation in pressure. The control signal variation shows that both controllers take similar control efforts.

C. Pressurizer Control Loop

1) Pressure Control Loop: The closed-loop system behaviour is studied for a disturbance in the surge flow rate. A -1kg/s perturbation is applied from $t = 50$s to $t = 100$s

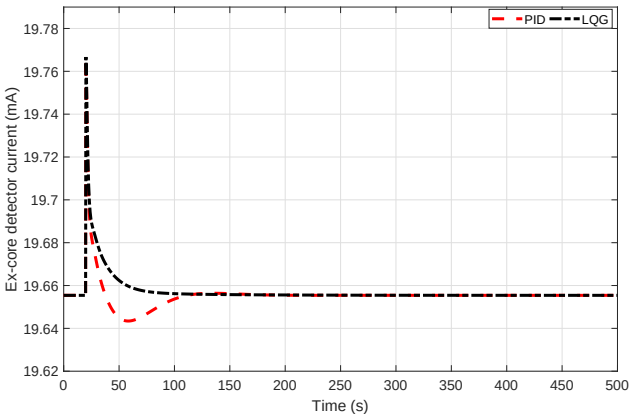

(a) Ex-core detector current.

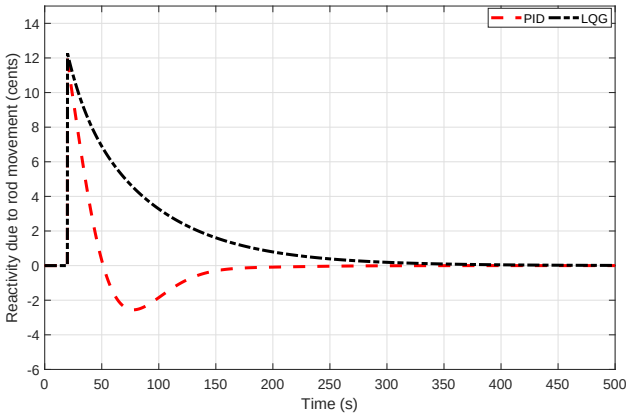

(b) Reactivity injected by rod movement.

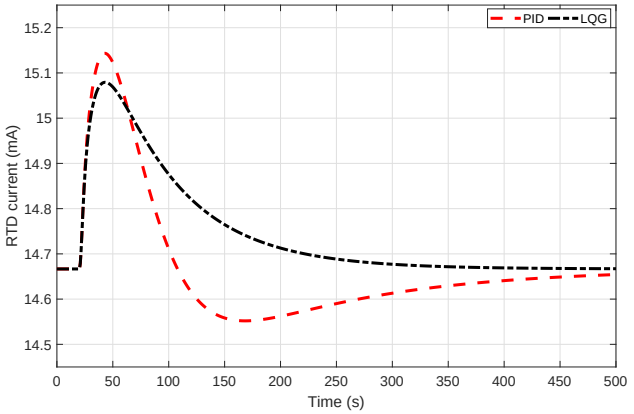

(c) RTD current.

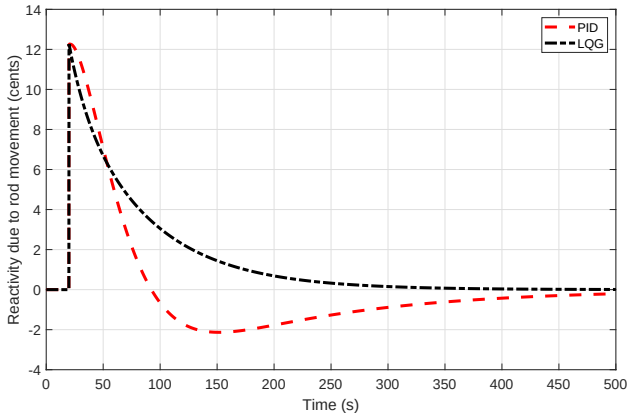

(d) Reactivity injected by rod movement.

Fig. 12: Response of reactor power loop controllers.

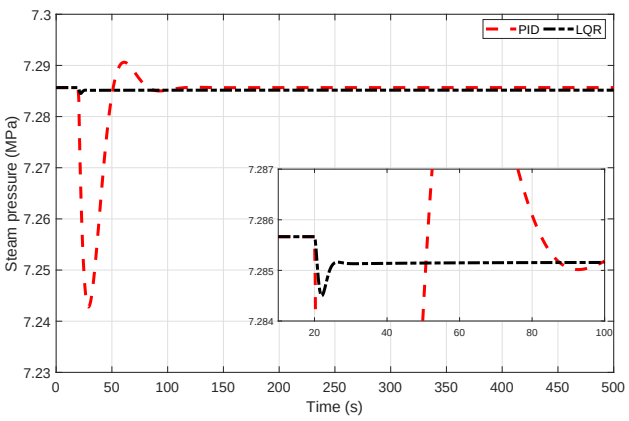

(a) Steam generator pressure.

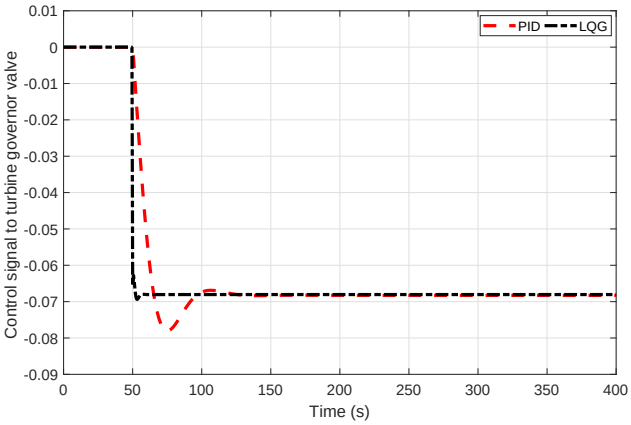

(b) Control signal to turbine governor valve.

Fig. 13: Response of steam generator pressure loop controllers.

and $+1$kg/s perturbation from $t = 100$s to $t = 150$s. In open-loop, it will cause the pressure to decrease and settle at a lower steady-state value. Whereas, in closed-loop, as the pressure goes below the reference, the heater control system gets actuated. The performance of the PI and LQG heater controllers is shown in Fig. 14a. The control signal variation of rate of heat addition is shown in Fig. 14b. Another perturbation with a rate of $+50$kg/s is applied from $t = 50$s to $t = 100$s and -50kg/s from $t = 100$s to $t = 150$s. The fast varying perturbation actuates the spray system and the spray valve gets opened. The performance of the PI and LQG spray flow rate controllers is shown in Fig. 14c. The rate of spray flow control signal variation is shown in Fig. 14d. In both simulations, the controllers act to reject the effect of disturbances. The LQG controller rejects the disturbance with lower variation in pressure and it is noted that both controllers make similar control efforts.

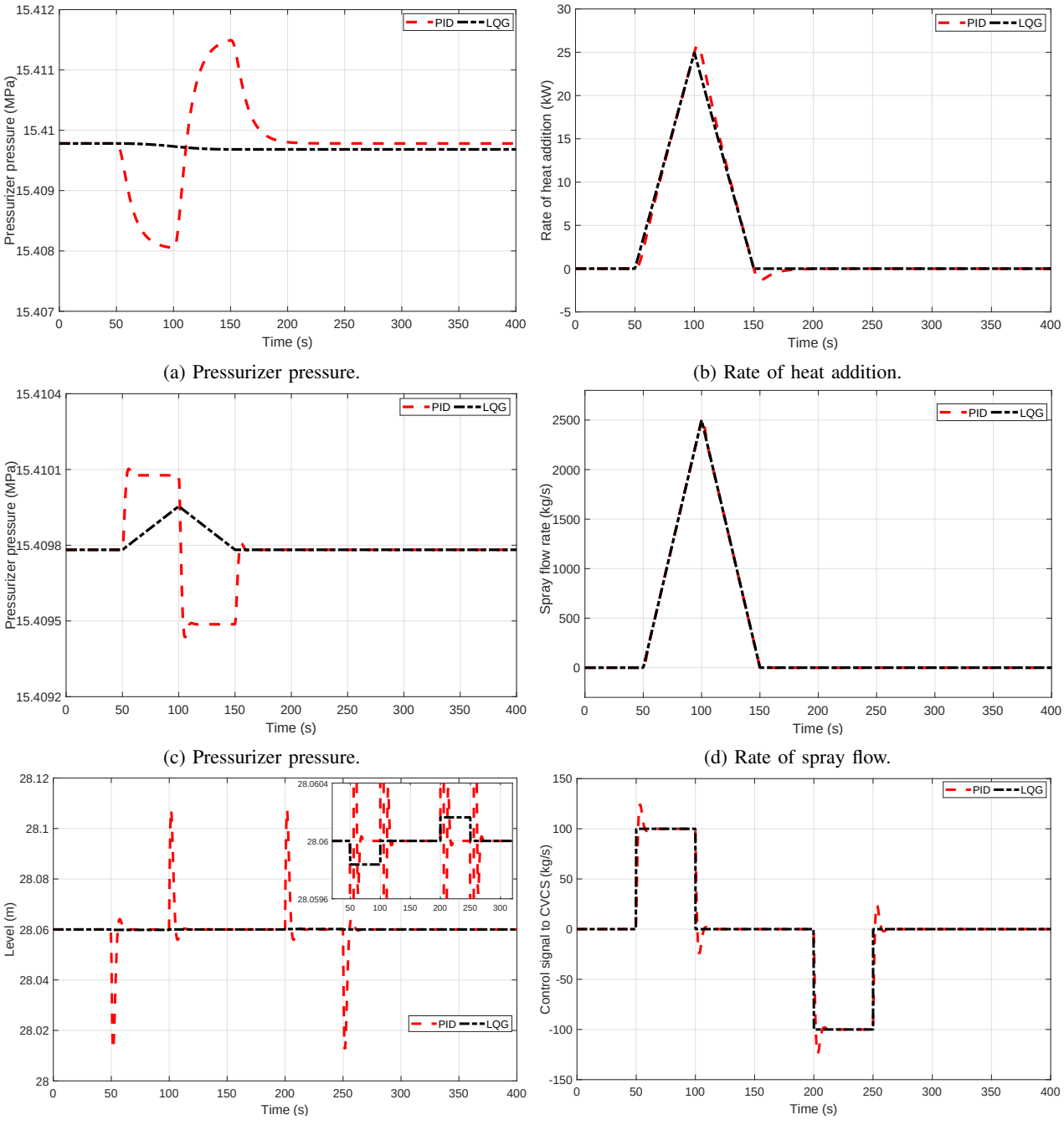

(a) Pressurizer pressure.

(b) Rate of heat addition.

(c) Pressurizer pressure.

(d) Rate of spray flow.

(e) Pressurizer level.

(f) Control signal to CVCS.

Fig. 14: Response of pressurizer loop controllers.

2) Level Control Loop: The performance of the pressurizer level controller is studied for a step disturbance in the flow rate. A step decrement is applied from $t = 50$s to $t = 100$s and a step increment is applied from $t = 200$s to $t = 100$s. The performance of the proposed PI and LQG level controllers is shown in Fig. 14e and 14f. It can be seen that the both controllers are able to reject the disturbance and maintain the level at its set-point. The LQG controller smoothly maintains the level whereas the PI controller produces overshoot and undershoot. Both controllers take similar control efforts as can be seen by the control signal variation.

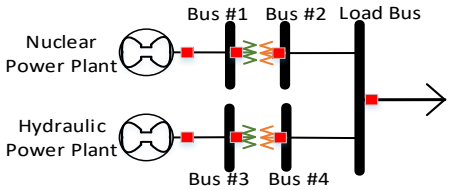

Fig. 15: Network model of an electric grid.

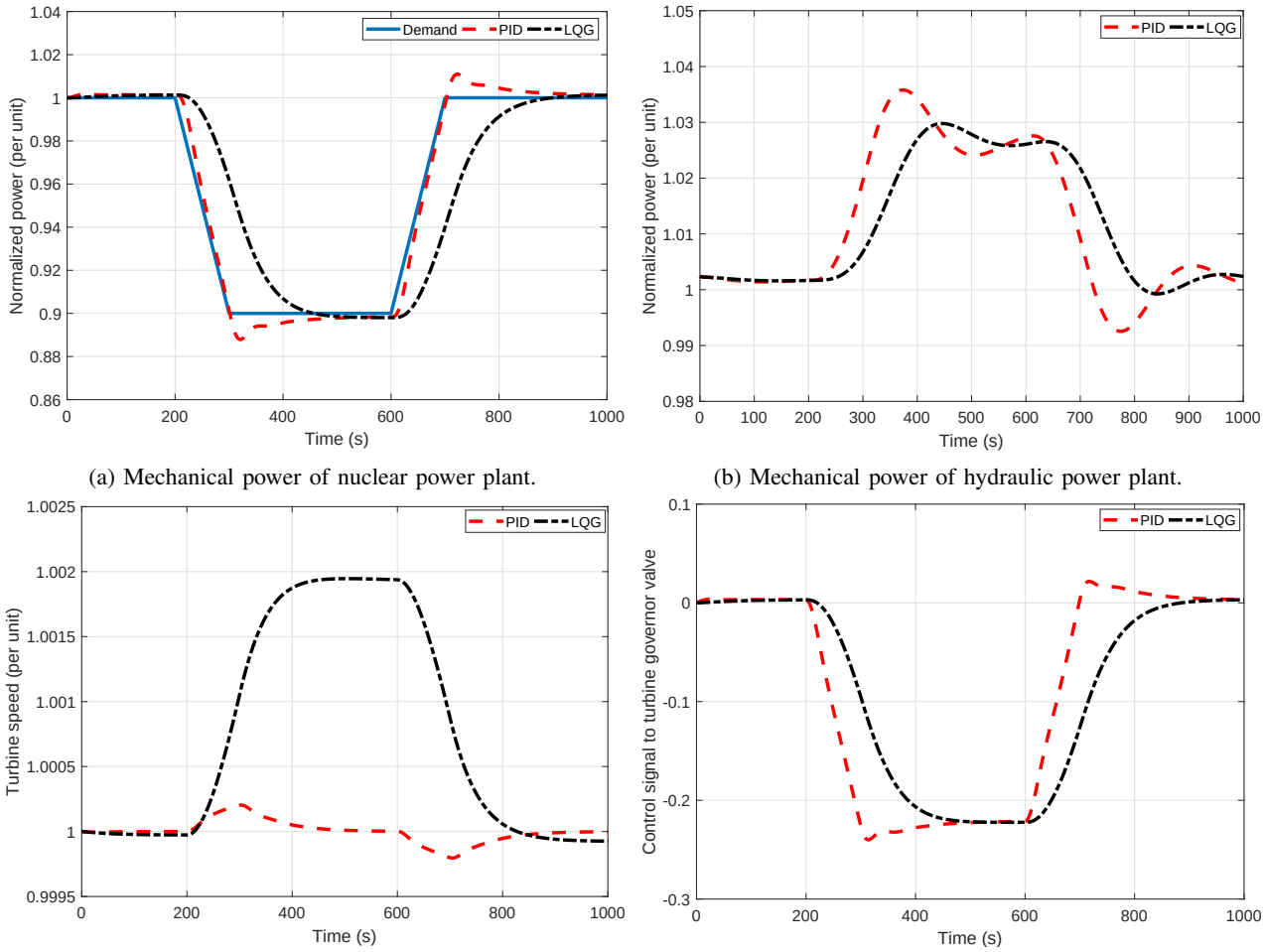

(a) Mechanical power of nuclear power plant.

(b) Mechanical power of hydraulic power plant.

(c) Turbine speed.

(d) Control signal to turbine governor valve.

Fig. 16: Response during load-following mode of operation.

D. Turbine Speed Control Loop

The performance of the turbine speed control loop is tested for load-following and load-rejection simulation. Fig. 15 shows the network model of an electric grid with two plants having a total electrical power generation capacity of 7.2 GW, including a nuclear power plant of 1.2 GWe capacity and a hydraulic power plant of 6 GWe capacity.

1) Load-Following Transient: A load-following transient is applied to vary the power output of the nuclear power plant. Initially, both plants are assumed to be operating at their full power. The load-following transient is applied as follows: For 200 s the desired power is maintained at 1.0 fractional full-power (FFP); then, it is changed to 0.9 FFP in 100 s and held at 0.9 FFP for the next 300 s; then, it is brought back to initial value in a similar manner. The performance of the proposed controllers during load-following mode of operation is shown in Fig. 16. It can be be seen that the turbine output from the LQG controller is steadily able to track the set-point variation whereas the PI controller is able to track the variation with peak overshoots. The mechanical power output of nuclear and hydraulic plants are shown in Fig. 16a and 16b, respectively. Due to reduction in power output from nuclear plant, the hydraulic plant increase the power output so as to keep the total power output constant. The variation in turbine speed and the corresponding control signal to the turbine-governor valve of the nuclear power plant are shown in Figs. 16c and 16d, respectively. It is noted that the PI control signal makes larger excursions than the LQG control signal.

2) Load-Rejection Transient: To simulate an emergency operation of a sudden load-rejection, the power output of nuclear power plant is brought down by 10%. Both plants are assumed to be in steady-state operation at 1.0 FFP. At $t = 200$ s, a sudden reduction of load to 0.90 FFP is assumed to take place at the nuclear power plant. The performance of the proposed controllers in tracking the load-rejection transient is shown in Fig. 17. Both controllers are able to handle the sudden step decrease in the load and are effectively able to track the set-point. The mechanical power output of the nuclear and the hydraulic plants are shown in Fig. 17a and 17b, respectively. With the LQG controller, the turbine output power tracks the load exhibiting an overdamped response and no overshoot, while the with the PID controller the turbine output tracks the load change with an oscillatory response and 3.6% overshoot. The settling time is similar in both cases. The hydraulic plant gives lower variations in the power output when the LQG controller is employed on the NPP. It is to be

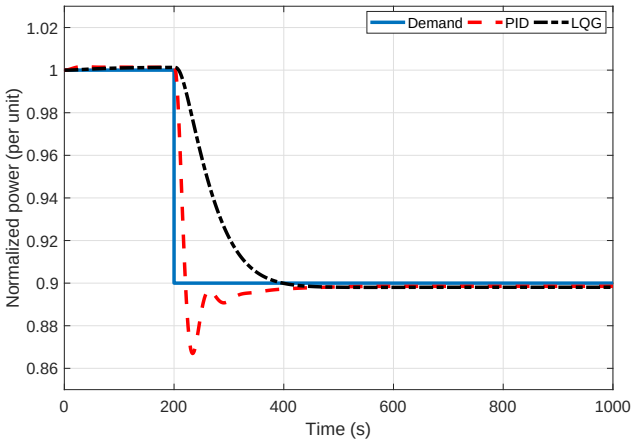

(a) Mechanical power of nuclear power plant.

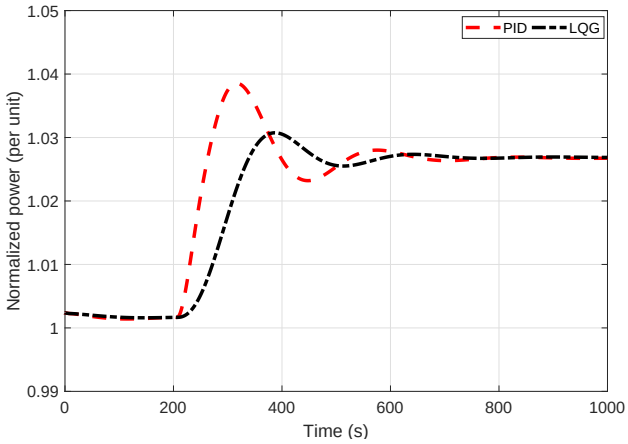

(b) Mechanical power of hydraulic power plant.

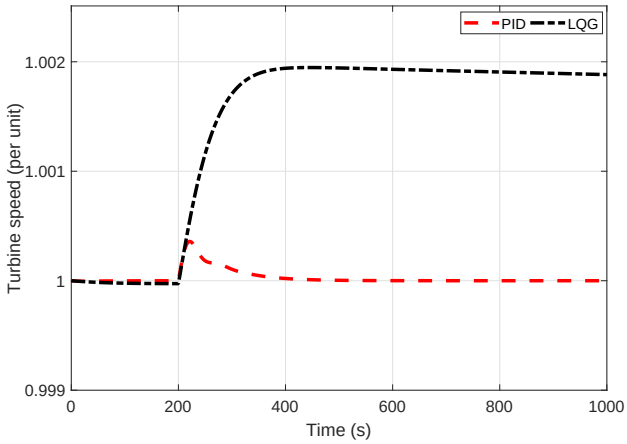

(c) Turbine speed.

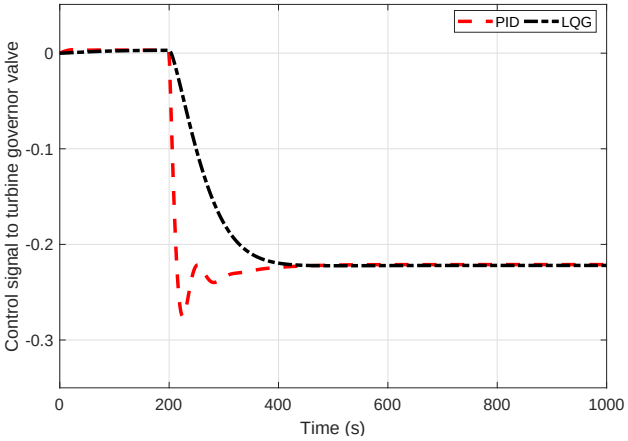

(d) Control signal to turbine governor valve.

Fig. 17: Response during load-rejection transient.

noted that the proposed PI and LQG controllers are operates on the NPP turbine. The variation in turbine speed and the control signal to the turbine-governor valve of the nuclear power plant are shown in Figs. 17c and 17d, respectively. The PI controller tracks the transient with large overshoot and takes more control efforts than the LQG controller.

IX. Conclusions

A non-linear mathematical model of a PWR-type nuclear power plant has been formulated for the purpose of control design and evaluation. The dynamics of actuators, sensors, core-neutronics, thermal-hydraulics, piping, plenum, pressurizer, steam generator, turbine-generator, condenser, and reactivity feedback systems have been represented in the model. The main contribution of the proposed work is to present a simple yet complete model of a PWR-type nuclear power plant suitable for control system design and simulation purposes. The response of the proposed model has been evaluated for different perturbations in the input variables. Further, various control loops have also been designed to study the closed loop response of the nuclear power plant. PI and LQG-based control strategies for reactor power, average coolant temperature, steam generator pressure, pressurizer pressure, pressurizer level, and turbine speed control loops have been formulated and implemented after careful tuning. The model has been validated against real plat data and a good fit has been obtained between plant data and model response. The open and closed loop response of the complete model have been discussed for different disturbances. The control system has been applied to assess load-following and load-rejection capabilities of the closed-loop plant in addition to the disturbance rejection capabilities in different loops. The effectiveness of the proposed work has been demonstrated using simulations in the MATLAB/Simulink environment. The proposed model provides an accurate representation of plant behaviour and is able to capture the important dynamics. It is easy to use and it forms a platform for future works on advanced controllers, observers, fault detection and diagnosis techniques in a PWR-type nuclear power plant.

X. Acknowledgement

The authors are grateful to Mr. K N V Sairam, Mr. T U Bhatt, and Mr. A K Mishra of Bhabha Atomic Research Centre, Mumbai, India for their valuable feedback.

The work presented in this paper has been financially supported under grants EP/R021961/1 and EP/R022062/1 from the Engineering and Physical Sciences Research Council.

REFERENCES

[1] J. J. Duderstadt and L. J. Hamilton, *Nuclear reactor analysis*. New York: Wiley, 1976.

[2] C. S. Subudhi, T. U. Bhatt, and A. P. Tiwari, "A mathematical model for total power control loop of large PHWRs," *IEEE Transactions on Nuclear Science*, vol. 63, no. 3, pp. 1901–1911, June 2016.

[3] A. P. Tiwari, B. Bandyopadhyay, and G. Govindarajan, "Spatial control of large pressurized heavy water reactor," *IEEE Transactions on Nuclear Science*, vol. 43, no. 4, pp. 2440–2453, 1996.

[4] H. Javidnia, J. Jiang, and M. Borairi, "Modeling and simulation of a CANDU reactor for control system design and analysis," *Nuclear Technology*, vol. 165, no. 2, pp. 174–189, 2009.

[5] J. D. Freels, *Modeling for Long-Term Power System Dynamic Simulation*. Master's thesis, University of Tennessee, Knoxville, 1978.

[6] M. J. Mneimneh, *Modular Modeling of a PWR System*. Master's thesis, University of Tennessee, Knoxville, 1984.

[7] M. R. A. Ali, *Lumped Parameter, State Variable Dynamic Models for U-tube Recirculation Type Nuclear Steam Generators*. PhD dissertation, University of Tennessee, Knoxville, 1976.

[8] J. G. Thakkar, *Correlation of Theory and Experiment for the Dynamics of a Pressurized Water Reactor*. Master's thesis, University of Tennessee, Knoxville, 1975.

[9] D. A. Botelho, P. A. D. Sampaio, C. M. Lapa, C. M. Pereira, M. de Lourdes Moreira, and A. C. de O. Barroso, "The IRIS pressurizer: Simulation of out-surge transients and optimization procedure to design scaled experiments," *Progress in Nuclear Energy*, vol. 50, no. 7, pp. 730 – 739, 2008.

[10] A. Pini, A. Cammi, L. Colombo, and A. B. Tigliole, "A non-equilibrium control oriented model for the pressurizer dynamics," *Progress in Nuclear Energy*, vol. 106, pp. 102 – 119, 2018.

[11] P. Wang, J. He, X. Wei, and F. Zhao, "Mathematical modeling of a pressurizer in a pressurized water reactor for control design," *Applied Mathematical Modelling*, vol. 65, pp. 187 – 206, 2019.

[12] T. W. Kerlin, E. M. Katz, J. G. Thakkar, and J. E. Strange, "Theoretical and experimental dynamic analysis of the H. B. Robinson nuclear plant," *Nuclear Technology*, vol. 30, no. 3, pp. 299–316, 1976.

[13] T. W. Kerlin, *Dynamic Analysis and Control of Pressurized Water Reactors*. Academic Press, 1978, vol. 14.

[14] S. E. Arda and K. E. Holbert, "A dynamic model of a passively cooled small modular reactor for controller design purposes," *Nuclear Engineering and Design*, vol. 289, pp. 218–230, 2015.

[15] ——, "Nonlinear dynamic modeling and simulation of a passively cooled small modular reactor," *Progress in Nuclear Energy*, vol. 91, pp. 116–131, 2016.

[16] M. Naghedolfeizi, *Dynamic Modeling of a Pressurized Water Reactor Plant for Diagnostics and Control*. Master's thesis, University of Tennessee, Knoxville, 1990.

[17] J. Wan, P. Wang, S. Wu, and F. Zhao, "Controller design for the reactor power control system of the advanced small pressurized water reactor," *Nuclear Technology*, vol. 198, no. 1, pp. 26–42, 2017.

[18] M. E. Pomerantz, C. R. Calabreseb, and C. Grant, "Nuclear reactor power and flux distribution fitting from a diffusion theory model and experimental data," *Annals of Nuclear Energy*, vol. 29, no. 9, pp. 1073–1083, 2002.

[19] D. Lathouwers, A. Agug, T. H. J. J. Van Der Hagen, H. Van Dam, C. C. Pain, C. R. E. de Oliveira, and A. J. H. Goddard, "Dynamics modeling and stability analysis of a fluidized bed nuclear reactor," *Annals of Nuclear Energy*, vol. 43, no. 1–4, pp. 437–443, 2003.

[20] W. C. Venter and E. C. Lamprecht, "Pebble bed micro model system identification," *Annals of Nuclear Energy*, vol. 46, pp. 1–10, 2012.

[21] C. Fazekas, G. Szederkenyi, and K. M. Hangos, "A simple dynamic model of the primary circuit in VVER plants for controller design purposes," *Nuclear Engineering and Design*, vol. 237, pp. 1071–1087, 2007.

[22] A. Gabor, C. Fazekas, G. Szederkenyi, and K. M. Hangos, "Modeling and identification of a nuclear reactor with temperature effects and xenon poisoning," *European Journal of Control*, vol. 17, no. 1, pp. 104–115, 2011.

[23] S. Das, S. Das, and A. Gupta, "Fractional order modeling of a PHWR under step-back condition and control of its global power with a robust PID controller," *IEEE Transactions on Nuclear Science*, vol. 58, no. 5, pp. 2431–2441, 2011.

[24] J. J. Sohn and P. H. Seong, "A steam generator model identification and robust H_∞ controller design with v-gap metric for a feedwater control system," *Annals of Nuclear Energy*, vol. 37, pp. 180–195, 2010.

[25] H. G. Kim, S. H. Chang, and B. H. Lee, "Pressurized water reactor core parameter prediction using an artificial neural network," *Nuclear Science and Engineering*, vol. 113, no. 1, pp. 70–76, 1993.

[26] F. Cadini, E. Zio, and N. Pedroni, "Simulating the dynamics of the neutron flux in a nuclear reactor by locally recurrent neural network," *Annals of Nuclear Energy*, vol. 34, no. 6, pp. 483–495, 2007.

[27] E. Zio, M. Broggi, and N. Pedroni, "Nuclear reactor dynamics on-line estimation by locally recurrent neural network," *Progress in Nuclear Energy*, vol. 51, no. 3, pp. 573–581, 2009.

[28] M. Boroushaki, M. B. Ghofrani, C. Lucas, and M. J. Yazdanpanah, "Identification and control of a nuclear reactor core (VVER) using recurrent neural networks and fuzzy systems," *IEEE Transactions on Nuclear Science*, vol. 50, no. 1, pp. 159–174, Feb 2003.

[29] M. V. de Oliveira and J. C. S. de Almeida, "Application of artificial intelligence techniques in modeling and control of a nuclear power plant pressurizer system," *Progress in Nuclear Energy*, vol. 63, pp. 71 – 85, 2013.

[30] H. Khalafi and M. S. Terman, "Development of a neural simulator for research reactor dynamics," *Progress in Nuclear Energy*, vol. 51, no. 1, pp. 135–140, 2009.

[31] M. Marseguerra, E. Zio, and P. Avogadri, "Model identification by neuro-fuzzy techniques: Predicting the water level in a steam generator of a PWR," *Progress in Nuclear Energy*, vol. 44, no. 3, pp. 237–252, 2004.

[32] V. Vajpayee, S. Mukhopadhyay, and A. P. Tiwari, "Multiscale subspace identification of nuclear reactor using wavelet basis function," *Annals of Nuclear Energy*, vol. 111, pp. 280–292, 2018.

[33] ——, "Wavelet-based on-line multiscale subspace identification of nuclear reactor," *IFAC-PapersOnLine*, vol. 51, no. 15, pp. 347 – 352, 2018, 18th IFAC Symposium on System Identification SYSID 2018.

[34] A. J. Gaikwad, R. Kumar, S. F. Vhora, G. Chakraborty, and V. V. Raj, "Transient analysis following tripping of a primary circulating pump for 500-MWe PHWR power plant," *IEEE Transactions on Nuclear Science*, vol. 50, no. 2, pp. 288–293, 2003.

[35] *PCTRAN Generic Pressurized Water Reactor Simulator Exercise Handbook*, ser. Training Course Series. Vienna: International Atomic Energy Agency, 2019, no. 68. [Online]. Available: https://www.iaea.org/publications/13463/pctran-generic-pressurized-water-reactor-simulator-exercise-handbook

[36] A. Prosek and M. Matkovic, "RELAP5/MOD3.3 analysis of the loss of external power event with safety injection actuation," *Science and Technology of Nuclear Installations*, vol. 2018, p. 6964946, 2018.

[37] E. Takasuo, "Modeling of pressurizer using APROS and TRACE thermal hydraulic codes," 2005.

[38] *Westinghouse Technology Course R-104P Manual*. US-NRC Technical Training Center, 2012. [Online]. Available: https://www.nrc.gov/docs/ML0230/

[39] A. H. Harvey, *Thermodynamic Properties of Water: Tabulation from the IAPWS Formulation 1995 for the Thermodynamic Properties of Ordinary Water Substance for General and Scientific Use*. NISTIR, 1998. [Online]. Available: https://www.nist.gov/srd/nistir-5078

[40] L. Wang, W. Sun, J. Zhao, and D. Liu, "A speed-governing system model with over-frequency protection for nuclear power generating units," *Energies*, vol. 13, no. 173, 2020.

[41] P. V. Surjagade, A. P. Tiwari, and S. R. Shimjith, "Robust optimal integral sliding mode controller for total power control of large PHWRs," *IEEE Transactions on Nuclear Science*, vol. 65, no. 7, pp. 1331–1344, July 2018.

[42] C.-T. Chen, *Linear System Theory and Design*, 2nd ed. USA: Oxford University Press, Inc., 1995.

[43] S. R. Shimjith, A. P. Tiwari, M. Naskar, and B. Bandyopadhyay, "Space–time kinetics modeling of advanced heavy water reactor for control studies," *Annals of Nuclear Energy*, vol. 37, no. 3, pp. 310 – 324, 2010.

[44] *Pressurized Water Reactor Simulator*, ser. Training Course Series No. 22. International Atomic Energy Agency, Vienna, 2005, no. 22/02. [Online]. Available: https://www.iaea.org/publications/6856/pressurized-water-reactor-simulator